LOW TEMPERATURE HALL MEASUREMENTS OF NEUTRON IRRADIATED SILICON CARBIDE

THESIS

Angelo M. Bonavita, Second Lieutenant, USAF

AFIT/GNE/ENP/04-01

DEPARTMENT OF THE AIR FORCE
AIR UNIVERSITY

AIR FORCE INSTITUTE OF TECHNOLOGY

Wright-Patterson Air Force Base, Ohio

The views expressed in this thesis are those of the author and do not reflect the official policy or position of the United States Air Force, Department of Defense, or the United States Government

AFIT/GNE/ENP/04-01

LOW TEMPERATURE HALL MEASUREMENTS OF NEUTRON IRRADIATED SILICON CARBIDE

THESIS

Presented to the Faculty

Department of Engineering Physics

Graduate School of Engineering and Management

Air Force Institute of Technology

Air University

Air Education and Training Command

In Partial Fulfillment of the Requirements for the

Degree of Master of Science in Nuclear Engineering

Angelo M. Bonavita, BS, EIT

Second Lieutenant, USAF

March 2004

AFIT/GNE/ENP/04-01

LOW TEMPERATURE HALL MEASUREMENTS OF NEUTRON IRRADIATED SILICON CARBIDE

Angelo M. Bonavita, BS, EIT

Second Lieutenant, USAF

Approved:

James C. Petrosky (Chairman)	19MAR04 Date
Larry W. Burggraf (Member)	19 Mar 04 Date
Robert L. Hengehold (Member)	19 Mar 04 Date

Abstract

The purpose of this research was to search for evidence of low temperature annealing from neutron irradiated 4H-silicon carbide. No features suggesting annealing were found below a temperature of 340K. Temperature dependant Hall effect measurements were taken over a range of 100K to 340K recording resistivity, carrier densities, and mobility. Resistivity was noted to increase with irradiation, and carrier densities appeared to decrease, while mobility appeared minimally affected by neutron irradiation. This suggests the creation of active acceptor defects decreasing carrier concentrations. N-type samples measured were 5mm x 5mm square with Nickel contacts, and irradiated to 10^{15} and 10^{16} n-cm/cm^3 of 1MeV equivalent neutron fluence. Suggestions for continuing research include using a probe station instead of wire connections to samples, use a large source current to minimize variance, and minimize cadmium shielding to reduce negative reactivity.

Acknowledgements

Many individuals contributed to the success of this project, and I would like to properly thank each of them:

First, I would like to thank LTC James Petrosky for helping me keep a calm optimistic attitude, and guiding me through the world of radiation effects;

Eric Taylor for his aid whenever a part went missing, and it had to be found or a replacement invented;

Rick Patton in the AFIT clean room for allowing me to complete my training and work promptly;

The nuclear research reactor team at Ohio State University especially Andrew Kauffman and Joe Talnagi;

AFRL sensors directorate, especially Larry Callahan who attached the original wires, and Tim Cooper who conducted Hall measurements;

Lastly, I need to thank my classmates in the GNE 2004 class, who lent me great amounts of support.

Angelo M. Bonavita

Table of Contents

List of Figures

List of Tables

Table Page

HALL MEASUREMENTS OF SURFACE DEFECTS IN NEUTRON IRRADIATED SILICON CARBIDE

I. Introduction

The Promise of Silicon Carbide

Just as silicon revolutionized electronics in the twentieth century, silicon carbide will change how we think about electronics in the twenty-first century. Silicon carbide (SiC) is a wide band-gap semiconductor, the material of choice for extreme environment electronics. Silicon carbide is attractive for use in high-temperature, high-power, high frequency, and highly radioactive environments. The United States Air Force is researching methods of exploiting the material to improve access, reliability, and lethality of military assets. This thesis proposes to look at the effects of neutron damage to silicon carbide.

Silicon carbide is attractive for use in high-temperature, high-power, high-frequency, and highly radioactive environments. Traditional silicon has a lifetime of 10 years in an environment of 100° C, and is unable to operate above 250° C [36,4]. SiC is expected to survive for a similar lifetime in an environment of 500° C and higher [36]. Additionally, silicon carbide's large breakdown electric field suggests excellent suitability for high-frequency applications [48]. McLean note survivability of SiC devices up to a neutron fluence of 10^{16} $\frac{n \cdot cm}{cm^3}$ [36]. With respect to primary damage caused by neutron irradiation, SiC is superior to silicon [26].

To the military, silicon carbide means easier maintenance, faster aircraft, and improved survivability for space-based platforms. Silicon carbide's high thermal

conductivity allows for device placement in engines decreasing troubleshooting time. SiC devices will reduce cooling requirements, making platforms lighter, increasing speed and decreasing mass budgets. SiC promises to "provide high power solid-state radars for future tactical systems" [9].

The USAF understands the potential of SiC devices and has devoted appropriate resources to developing the material. From 1992 to 1996 the USAF established the consortium for the development of silicon carbide for electronics applications, a group to study SiC supporting research at US Universities [9]. The Air Force Research Laboratory (AFRL) currently studies advanced contacts on SiC as the promise of SiC based devices is hindered by the limitations of device contacts. Multiple theses completed at the Air Force Institute of Technology concentrate on characterizing the properties of SiC.

The interest in silicon carbide surfaces in particular is the result of device vulnerabilities at junctions. For junction devices, ionizing radiation incident on active junctions results in an increase of carriers. For metal oxide semiconductor (MOS) devices, ionizing radiation results in charge trapping at the oxide-semiconductor junction [17:134]. Non-ionizing radiation, caused by interactions with heavy particles leads to displacement damage such as point defects in the crystal structure. These defects in the lattice cause charge carriers to scatter, decreasing mobility and increasing resistivity.

Objective

This experiment attempts to examine the annealing behavior of the surface of neutron damaged 4H-SiC over a temperature range from 100 K to 350 K. Characterization of the post-irradiated surface's electrical properties will aid in identifying modes of failure. By comparing temperature dependency of mobility in

irradiated and non-irradiated samples, displacement damage can be identified by observing recovery of resistivity, mobility, or carrier concentration.

Paper Organization

The following thesis is divided into supporting theory, experimental procedure, results, and conclusion. Chapter II introduces the theory behind models of conduction, the crystal structures of SiC, and a primer on Hall Effect measurements. Chapter III discusses the experiment including equipment, the planned experiment, and the changes that were required. The results from the experiment are presented and analyzed in Chapter IV. Chapter V extracts the most fundamental results, and proposes courses of action based upon knowledge gained.

II. Theory

Devices made from silicon carbide are more radiation tolerant than traditional silicon devices, making SiC attractive for use in the space and nuclear reactor environments. Both environments are filled with higher energy particles than normally found on the earth's surface. The next section describes how heavy, neutral particles induce damage to SiC.

Heavy Particle Interactions with Matter

Heavy Particles, such as neutrons, protons, and alpha particles, can impart enough energy through collisions to remove an atom from its position in a crystal lattice, creating a point defect. These defects are often called Frenkel pairs, which are a pair of simple defects – a vacancy and an interstitial [17:73]. Frenkel defects can create additional energy levels within the band gap, resulting in trap sites [46:11]. Heavy particles transfer only a fraction of their kinetic energy in a single collision and below certain energies, a particle cannot impart enough energy to cause a displacement. Equation 1 describes the relationship between the mass of both particles, the energy of the incident particle, and the maximum fraction of energy imparted in the collision. The first atom hit in the lattice by a particle is often referred to as the primary knock-on atom (PKA). The PKA often absorbs enough energy to create many secondary displacements in the lattice. Equation 1 also describes the maximum fraction of energy imparted to a secondary atom by the PKA.

$$\frac{Q_{\max}}{E_n} = \frac{4mM}{(m+M)^2} \text{ [54:213]} \qquad (1)$$

where, m, M ~ Masses of the particles involved, and

Q_{max}/E_n ~ Fraction of Energy imparted to PKA.

Given a neutron with kinetic energy E, a maximum of 0.133E is imparted to a silicon atom, and 0.284E to a carbon atom as calculated through use of (1). The threshold energy for an incident neutron, below which displacement is unlikely, is 10 keV [17:73]. While a neutron creates only a small number of PKAs, each PKA has the potential to create thousands of secondary defects within the lattice.

The Kinchin-Pease model of defect formation states that the number of defects is proportional to the energy of the PKA [17]. Also, the number of Frenkel pairs is proportional to the energy given to the PKA [17:73]. Using (1) again, we find that an atom can impart up to all of its energy to another atom of the same kind. Since, an atom can impart all of its energy, a 40 eV PKA can produce up to 1 defect. By the Kinchin-Pease model, that means a 133 keV PKA can create more than 3200 defects in SiC.

A particle only imparts the maximum amount of energy during a head-on collision. However, it is more likely that a collision will occur at another angle of attack. The energy transferred to an atom by a neutron is more generally described by equation 2.

$$\Delta E = \frac{4A}{(1+A)^2}\sin^2\frac{\theta}{2} \text{ [17:72]} \qquad (2)$$

where, E ~ Energy of neutron,

A ~ Atomic Mass of Target Atom, and

θ ~ Incident angle of attack.

Since the incident angle of attack for a particular collision is unknown, the average energy imparted is used over a large quantity of collisions. The average energy transferred (Q_{Ave})in a collision is accepted to be half of the maximum energy as denoted in equation 2. It is this energy that is the quantity of interest for dose calculations.

$$Q_{Ave} = \frac{1}{2} \cdot Q_{\max} \tag{3}$$

Electrons and gamma rays often do not transfer enough energy to create a Frenkel pair owing to their lower momentum, and because of this a neutron displaces a thousand times more atoms than an equivalent energetic electron [17:77]. Therefore the effects of electrons and gamma rays will be ignored in this study.

The dose to silicon carbide for the neutron flux of the reactor can be estimated by calculating the "first-collision" dose to the SiC for all neutrons with E > 10 keV [54:371, 17:73]. The first-collision dose sets a lower bound for the dose because it assumes that the neutron escapes the system before interacting more than once. This is a good estimate for systems where the thickness is much less than the mean free path length of the neutron. While reactors have different neutron energy distributions, comparisons to other radiation environments can be made by normalizing the fluence to a 1 MeV equivalent fluence. An example of finding 1MeV equivalent fluence is supplied in Appendix B.

Silicon carbide can survive a higher neutron dose than silicon due to stronger molecular bondings. The amount of energy required to free an atom from the lattice differs based on the atom and the geometry of its bonds. It takes about 40eV of energy to cause a displacement in SiC. Table 1 exhibits the amount of energy required to free a

silicon or carbon atom in specific planes of hexagonal silicon carbide. For comparison, a silicon atom in a silicon lattice requires only 13-20 eV to be displaced [26].

Table 1: Displacement Energy for Si & C atoms in the different crystal plans of SiC. Compiled from [45].

Plane	*Silicon (eV)*	*Carbon (eV)*
001	30 - 35	35 - 40
111	35	20 - 25
110	80 - 85	30

Defects in crystal structures can be removed through annealing. The two basic forms of annealing are isochronal and isothermal [17:80-84]. Isochronal annealing studies a range of temperatures to find the specific temperatures at which defects become mobile, returning to a normal lattice position. Isothermal annealing studies the time dependent change in properties at a specific temperature. For this study, in order to identify if annealing is occurring below 250° C, an isochronal annealing study was accomplished. In traditional silicon, Holmes-Siedel notes that the only annealing that occurs at temperatures below 200° C is at the semiconductor's surface [17:83]. This data should lend to support the possibility of similar annealing in silicon carbide.

Kronig-Penney Model of Conduction

Columbic force is the driver that shapes crystal structures. The Kronig-Penny model crudely models the Coulombic potential in a lattice as a periodic square wave [35:321]. This one-electron approximation assumes that the random interactions of other electrons in the lattice sum to zero, so that the periodic potential is all that remains. Others have simplified this model to represent the potential by periodic Dirac delta functions [14:200]. In either case, it is the periodicity of the potential yielding useful information. The solution of the Schrödinger equation with these periodic potentials leads

to bands of allowed and forbidden energy states. While not a precise approximation of the potentials felt in a crystal, the Kronig-Penney model has shown itself to be a useful tool. The Kronig-Penney models states that if the periodic structure is interrupted with a defect, the electrical properties will change.

A charge carrier traveling through a crystal with no defects would continuously accelerate under the influence of an electric field. However, this behavior is not observed. Instead crystals have many types of defects that act as scattering points for carriers. Defects create allowable states within the bandgap, trapping minority carriers from conducting. As defects in a crystal increase, conductivity decreases. The diversity of SiC polytypes increases the difficulty of describing the material in general as each crystal structure leads to slightly different electrical properties.

Silicon Carbide

Silicon carbide has been the subject of study for many decades. The first studies were done at the beginning of the twentieth century, but getting high purity crystals was a problem for a long time. In the 1980's research quality 6H-SiC became available commercially, followed by 4H-SiC in the 1990's. Due to availability, most research has concentrated on these two polytypes, preferring 4H owing to its larger bandgap.

Crystal Structures

Silicon carbide has many different polytypes. Polytypism is a one-dimensional form of polymorphism where the closest packed layers are similar, and crystals vary in the pattern of stacking layers [48]. While nearly 200 polytypes of SiC have been identified, only a few have the attention of researchers.

Silicon carbide lattice structures fall into three main types; Cubic (C), Hexagonal (H), and Rhombic (R). The stacking sequence of a polytype is usually described in Ramsdell or ABC notation, where each layer arbitrarily identifies a similar layer. The number preceding the letter C, H, or R describes the number of stacks in the pattern followed by a letter describing the crystal structure [42:138]. Only one cubic structure exists for SiC, and it is referred to as both β-SiC and 3C-SiC. β-SiC possesses the common zinc-blende lattice structure with the stacking pattern of ABC. The two most common hexagonal types are 6H and 4H SiC. 6H-SiC has an ABCACB stacking pattern, and 4H-SiC has an ABAC stacking pattern. Hexagonal and rhombic SiC are sometimes collectively referred to as α-SiC.

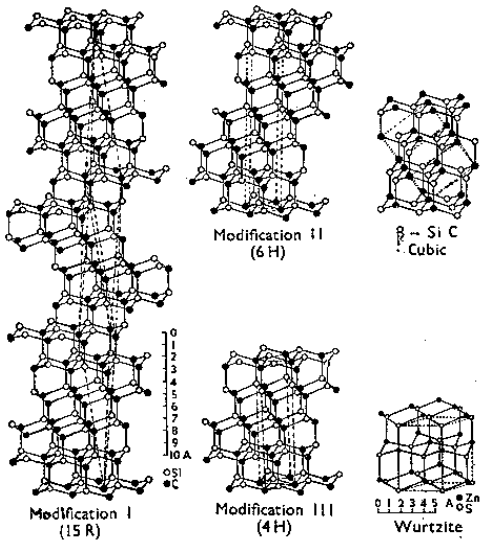

Figure 1: Structure of Common SiC Polytypes. Source [42:148]

Each crystal lattice of SiC has a unique bandgap that ranges from 2 to 4eV. 4H-SiC is the preferred crystal for researchers because its bandgap is larger than 6H-SiC.

Activation Concerns

Silicon carbide interests nuclear researchers in particular due to its low neutron absorption cross section. Silicon and carbon both possess small neutron absorption cross sections. Additionally, most silicon and carbon atoms must absorb 2 or 3 neutrons before becoming an active isotope. When silicon activates as Si-31, it decays quickly to a stable isotope of phosphorous. This characteristic can be used to dope SiC with silicon through a process known as neutron transmutation doping (NTD). The activation of SiC comes mostly from C-14, which has a long half-life of 5715 years. For the reason of low activation, SiC composites are being developing as structural materials for possible nuclear fusion reactors. After 30 years of operation in a fusion reactor, SiC could be safely discarded by shallow burial.

For this research, SiC's low activation potential means that the main activation concern stems from dopants, ohmic contacts, and wire bonds. Nitrogen and aluminum are the dopants for n- and p-type SiC respectively. Nitrogen possesses a small absorption cross section, decaying quickly to oxygen, and is of little concern. Aluminum also decays quickly, to silicon. Ohmic materials selected were nickel, aluminum, and titanium for reasons connected to ability to form a good contact.

Of the mentioned ohmic contact materials, none pose a potential of causing an activation problem. While $2/3$ of nickel will transmute to Ni-59 with a half-life of 7600 years, it decays by electron capture and only emits a neutrino. While Al activates more frequently, it decays quickly becoming insignificant within an hour.

While the creation of low resistance ohmic contacts drove the selection of contact material, activation was the driving force in selecting wire material. Potential materials

were compared using neutron absorption cross sections, and assuming transmutation to the n+1 isotope. By making this assumption, the (n,p) reaction was ignored. Ignoring other nuclear reactions underestimates total activation. Table 2 contains common elements used in electronics, with cadmium listed since it is often used to absorb lower energy neutrons. Elements with "Mostly Stable" listed under half-life need to capture two or more neutrons before they transmute into a radioactive isotope. The daughter products of all the listed elements are stable. Silicon and carbon both rarely transmute to an active radioisotope. When they become active, only C-14 maintains a high activity for a significant time, as Si-31 has a half-life of 2.6 hours.

Table 2: Thermal Cross sections and Half-Lives of elements common in electronics. Compiled from [2:68, 43]

Element	Thermal Crossection [barns]	Half-Life (after n-absorbtion)
Cadmium	2870	Mostly Stable
Silicon	0.14	Mostly Stable
Carbon	0.0035	Mostly Stable
Nickel	4.1	Mostly Stable
Nitrogen	1.67	Mostly Stable
Aluminum	0.217	2.25 min
Titanium	5.14	Mostly Stable
Gold	98.7	2.7 days
Indium	87	54 min

Gold and indium are elements common for wire bonding. The combination of a relatively large thermal absorption cross section and a 2.7 day half-life make gold undesirable for use in this project. Since a wire bonder makes wires along with contact bonds, a significant amount of gold may be used between all of the samples. If the gold is activated above permitted shipping levels, it may take up to a month before the samples could be retrieved. Indium also has a large thermal cross section, but its short half-life means that its activity the following day would be greatly reduced. However, indium has

a melting point of 156° C (429 K), which makes it undesirable for annealing to 200° C. A nickel / silver wire was finally chosen for wires on the samples.

Contact Formation

The ability to make effective ohmic contacts for silicon carbide is a major research area. All of the benefits of a high-temperature, high-power semiconductor are lost if the contacts cannot survive the environment. Some researchers describe the formation of good contacts as critical to the future of SiC devices.

Contacts at metal/SiC interfaces are either a Schottky (rectifying) contact, or an ohmic contact. A Schottky contact resembles the behavior of a diode, rectifying the current to pass preferentially in one direction. Ohmic contacts behave like resistors, increasing current flow proportionally with increased applied voltage. An ohmic contact is produced when the Schottky Barrier Height (SBH) is minimized. For this project, it is important to make contacts with ohmic behavior and low resistance.

For a long time, nickel has been the material of choice for good ohmic contacts on n-type silicon carbide. It was initially believed that the formation of Ni_2Si was the reason good contacts formed. The Ni - Si reaction separates the SiC leaving behind unreacted carbon, and was a concern for use in a high temperature environment [31]. The fear was that the carbon may bond with another material and degrade the contact. Studies show that Ni_2Si forms at much lower temperatures than the annealing temperature needed for contact formation [29]. In most cases, annealing temperatures above 900°C are needed to make low resistance ohmic contacts, with the exception of highly doped samples [48]. One study notes a significant improvement in resistance by annealing to 1000° C. However, Ni_2Si forms as low as 500° C. Studies of the unreacted carbon suggest that

graphitization of the material was the driving force behind ohmic contact formation [30]. It was found that graphite formed at temperatures of 900° C, very close to the necessary annealing temperatures. It was also found that materials that act as graphitic catalysts, such as Ni and Co, make good ohmic contacts on n-type SiC. Lu claims that Ni is used for ohmic contacts on n-type material not because we understand why it is a good choice, but only that it works. He comments that Ni, as well as Co, make good ohmic contacts because they are excellent catalysts for graphite formation in n-type SiC [30]. In another paper, Lu points out the silicides were once believed to be the source of ohmic contact formation, but the annealing temperature to form a silicide does not coincide with the temperature to form an ohmic contact [29].

While good contacts are easily fabricated for n-type SiC, it is very difficult to make suitable ohmic contacts for p-type SiC. Successful ohmic contacts have only been formed on highly doped (10^{18} cm^{-3}) samples. Ohmic contacts normally form by bonding a metal possessing a work-function equivalent to the electron affinity of the semiconductor. However, no known metal possesses a work function equivalent to 6eV, the electron affinity for p-type SiC, and thus a Schottky contact will always form. However, contacts can be made where electrons tunnel through the barrier in an ohmic manner. For the past few years, much research has been conducted on making effective ohmic contacts for silicon carbide.

Finding a suitable material remains a difficult task. Aluminum, a common dopant for p-type SiC, was recognized as having electrical properties suitable for good ohmic contacts. Aluminum has a low melting point, which is not suitable for use in high temperature applications. Titanium was added to aluminum to increase the melting point.

The AFIT labs have traditionally used an Al/Ti alloy consisting of 90% Al and 10 Ti% (90/10) for SiC contacts. However, a study on optimizing titanium content in the alloy found that using a 70/30 mixture improves resistivity, and increases reproducibility significantly [10]. A morphological study of 70/30 contacts found that the Al/Ti alloy contained a liquid phase that "spiked" into the material [39]. The 90/10 alloy resulted in a few long spikes, while the 70/30 resulted in shorter spikes with two orders of magnitude more abundance. The conclusion of the study was that the addition or subtraction of a spike in the 90/10 alloy lead to a much larger variance, and explained the difficulty of reproducing results with that mixture. The size of the 70/30 spikes was 65 nm maximum in depth.

Hall Effect Measurements

In 1879, as a master's student, Edwin Hall discovered the phenomena now known as the Hall effect. Hall noticed that when a conductor was exposed to a magnetic field oriented perpendicular to the current through the conductor, a voltage appeared across the height of the conductor. This phenomenon is related to the Lorentz force, as all of the carriers through the conductor are experiencing a $q\vec{v} \times \vec{B}$ force as they traversed though the device as depicted by Figure 2. Hall described the effect as "pressing electricity."

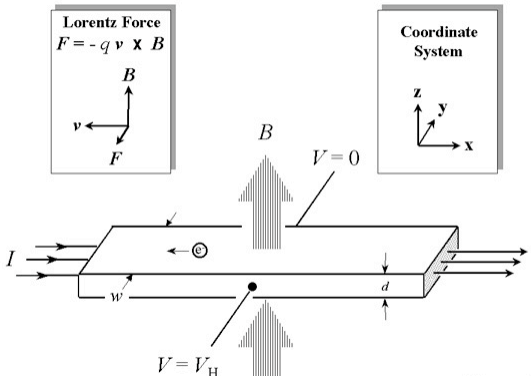

Figure 2: Hall effect in a planar bar. A current is run perpendicular to an external magnetic field, resulting in a force on the carrier. Source NIST [41]

While Hall used metal for his experiments, Hall effect techniques prove very helpful in the characterization of semiconductors, and shall be applied in this experiment to describing the mobility of neutron irradiated silicon carbide.

Initially, the Hall effect was used to describe the resistance of a particular material. Eventually, resistance was no longer considered a characteristic of a particular material, since values were geometrically dependent. Resistance was replaced as a characteristic property by resistivity. Resistivity quantifies the difficulty of a carrier to move through a material [41].

Resistivity is not independent of other material properties, and varies due to changes in carrier concentration in a material. Resistivity (ρ) is now denoted as a function of carrier mobility (μ_c), carrier density (n), and carrier charge (q) as related in equation 4.

$$\rho = \frac{1}{\mu_c n q} \tag{4}$$

Since carrier density varies with temperature, resistivity is also implicitly dependent on temperature. Thus, for this study it is important to characterize temperature dependent changes in resistivity to identify damage dependent changes in resistivity.

Hall effect measurements now aim at measuring mobility as a material's intrinsic electrical property. For comparing different materials, their mobility should be compared [41]. Hall effect measurements measure the Hall mobility of the material, and can be related to the conduction mobility by the relation:

$$\mu_H = \frac{3\pi}{8}\mu_c \approx 1.18\mu_c \tag{5}$$

Mobility, while being unique to a material, differs based on the crystal plane of the conduction medium. Mobility, thus is a second rank tensor differing in direction [51]. Since mobility is only compared as a scalar value, it is implied that this value is an average over the entire crystal.

There are two common methods of taking Hall effect measurements, the Van der Pauw method, and the Hall bar method. The Hall bar method requires a special geometry, while the Van der Pauw method can be used with almost any geometry. Due to the added complexity of creating a Hall bar geometry, the Van der Pauw method was used in this study. The Van der Pauw method combines 4 point Van der Pauw resistivity measurement with Hall measurements to determine mobility.

Hall measurements are particularly suited for studying surface defects. By applying a strong magnetic field, charge carriers are confined to a thin region of material. Since pre-knowledge of the depth is necessary, a thin conduction layer is required, and is accomplished by using samples possessing a thin epitaxial layer.

III. Experiment

This study was accomplished in four phases, equipment setup, sample fabrication, device irradiation, and temperature dependent measurement.

Equipment Setup and Testing

The first priority of this project was setting up and testing the measuring equipment. The Keithley system 110 was recently moved from another laboratory in the school. While minimal documentation was included with the system, the manuals for most components have been located on their manufacturers' respective website. The system components are listed in Table 3. The system depicted in Figure 3, contains a Walker-Scientific Electromagnet, and is controlled by a computer program over a general programming interface bus (GPIB).

Table 3: Equipment List for Keithley System 110

Make	*Model*	*Name*
Keithley	617	Electrometer
Keithley	196	Voltmeter
Keithley	---	Buffer Amplifier
Keithley	706	Scanner
Keithley	220	Current Source
Lakeshore	DRC-91CA	Coolant Controller
Walker-Scientific	---	Electromagnet
Walker-Scientific	MG-3D	Gaussmeter
Walker-Scientific	---	Current Controller

The system can be controlled either manually or by computer program. Manual operation requires opening and closing channels on the scanner in order for a particular device to have access to the sample from the quad buffer amplifier. Unfortunately,

documentation for which channels connect to which devices exists only in the form of a circuit diagram.

A computer program written by Keithley in QBasic and modified at AFIT was supplied with the system. The computer controller communicates to the system using a general programming instrument bus (GPIB) or IEEE 488 bus.

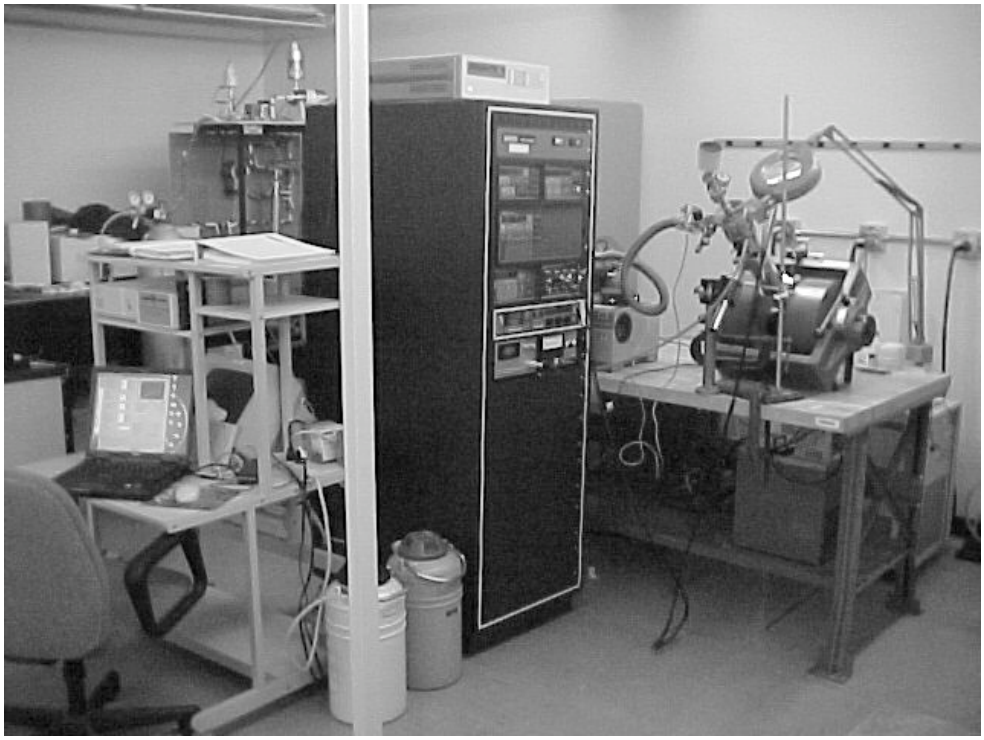

Figure 3: Keithley System 110

The measuring equipment, which had not been used for some time, required extensive assembly and troubleshooting to return to working order. Due to the time required, troubleshooting was accomplished in parallel with fabrication and irradiation. The greatest impediment was the lack of documentation stating changes in the system from its factory delivered state. Three major problems are worth discussing – computer, buffer, and power source.

The original documentation suggests running the supplied SYSTST program when first setting up and testing the system. However, all programs executed with the supplied computer failed with an error stating the bus could not be initialized. This complicated troubleshooting because the system manual suggests not attempting to manually operate the system until familiarity with computer controlled operation is achieved. As such, the manual reads as a programming guide, with no information about how to go about manual operation.

Difficulty launching the original Keithley program lead to the development of an in-house Visual Basic based program. The new program was written in the time span of a month, not allowing enough time for error checking code to be fully implemented. The code's modular format permits future users to easily develop new interfaces without having to redevelop the entire package.

The original design of the System 110 supplied power to the quad amplifier buffer through the scanner. The buffer had been modified to be powered with an external voltage source. The required power source must be able to supply both positive and negative polarity, sourcing –15V low, and simultaneously 15V high. This supplies power to the unity gain amplifiers required for high resistance testing. Fortunately, the SiC devices were of low enough resistance to use the low resistance terminals.

After successfully measuring a voltage drop across a resistor with a known applied current, the magnet was to be tested. Following the schematics supplied by a Walker-Scientific applications engineer, it was determined that a coolant flow safety was

not electrically closing as designed. Permanently shorting the circuit until the proper part could be ordered offered a temporary solution.

Sample Fabrication

Fabrication included cutting, cleaning, and forming ohmic contacts. Cutting samples into an optimal geometry can minimize errors in Van der Pauw measurements. Cleaning the sample removes impurities that can affect the creation of a good contact. While good contacts can be made easily for n-type SiC, it is very difficult to make good ohmic contacts for p-type SiC. Wiring was connected prior to irradiation to minimize heating. Due to the unique circumstances, of this experiment, traditional wiring techniques were not acceptable, and proved challenging.

Sample Cutting

The different methods for Hall effect measurements demand different geometries of use. The Van der Pauw method used in this experiment can be executed with an arbitrary geometry. However, in order to use derived equations, and minimize error, there exist recommended geometries.

NIST recommends use of a “cloverleaf” geometry as depicted in Figure 4. However, lithography methods must be used in order to develop this complex design. Satisfactory results can be obtained using a square geometry, with negligible loss in accuracy.

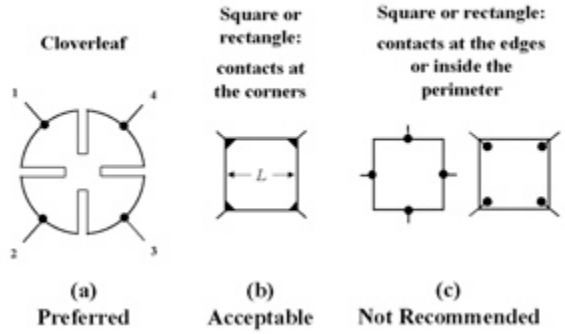

Figure 4: Recommended Geometries from NIST for use with Van der Pauw style Hall Measurements. Source [41]

In order to ensure accurate data a sufficient number of samples must be measured. Jones' results from a previous thesis suggest that sample deviation for n-type samples was only 3% error while deviation of p-type samples was about 10% [20, 54-57]. Small sample statistics can be used to determine the minimum number of samples required for this study. Equation 6 was used to determine the minimum number of samples required for the desired statistics.

$$I = \frac{t(\nu)s}{\sqrt{N}} \tag{6}$$

where

I	~	confidence interval,
t	~	t student distribution,
ν	~	degrees of freedom = N-1,
N	~	number of samples, and
s	~	sample standard deviation.

Since the n-type SiC has a small variance, only 4 samples per fluence are required for 95% confidence of a 5% interval. P-type SiC has a much larger variance; a 90% confidence interval with a resolution of 10% was chosen to keep the sample size to a

manageable 5 samples per fluence. Over the range of 4 fluences, 20 samples from each wafer will satisfy requirements for this thesis.

Several wafers of 4H-SiC were purchased from Cree Inc in support of a previous thesis. Enough previously cut, but otherwise untouched, remained from that experiment to be used with this study with satisfactory statistics. Figure 5 shows a 5mm x 5mm sample with a penny for scale.

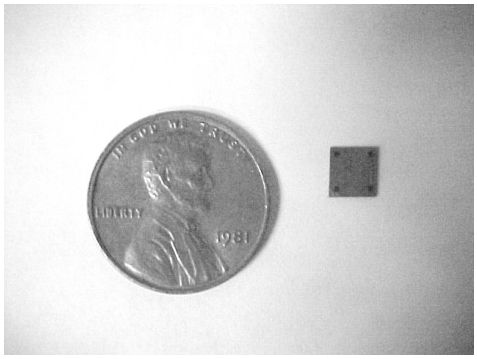

Figure 5: Example 5mm x 5mm Sample.
Note that sample is roughly the size of Lincoln's head on a penny.

A few samples had to be cut by a wafer saw to get the desired 5mm x 5mm square dimensions. On the day of the cut, the wafer saw did not completely cut through the material, producing only a deep grove. Excess material was removed by being snapped at the groove. While this procedure is common for silicon, it can lead to cracking in silicon carbide due to a non-planar crystal boundary. Figure 6 depicts the groove left on one sample, and a crack caused on another sample due to snapping off the extra material.

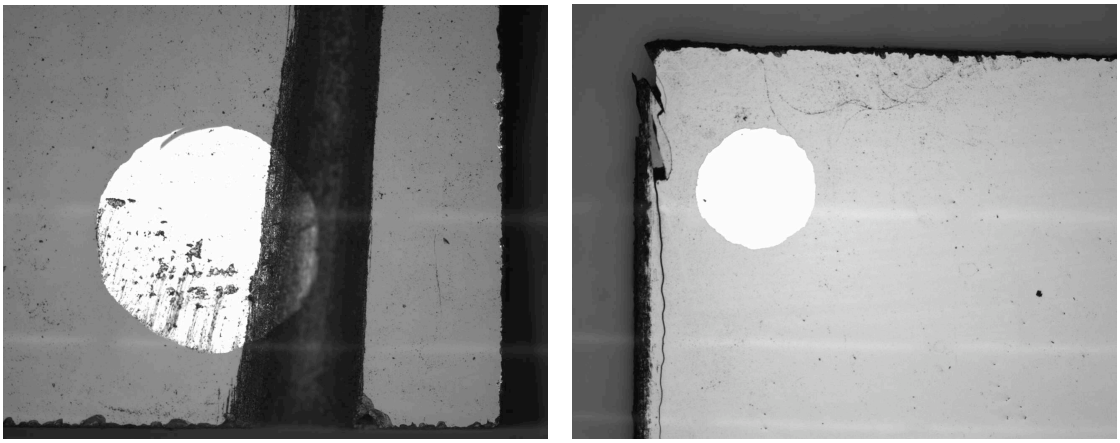

Figure 6: (Left) A groove cut into a sample. (Right) A crack caused by snapping off excess material.

While enough pre-cut samples existed to meet minimum desired statistics, a certain amount of attrition should have also been factored into the statistics. Over the course of the project, several samples were either lost, did not display ohmic behavior, or were damaged before a measurement could be taken. As a result, the number of samples measured was less than the number required as calculated above. After ensuring that the samples possessed the desired geometry, the samples were cleaned in preparation for deposition of the ohmic contacts.

Device Cleaning

The purpose of cleaning is to remove any impurities that may have occurred from handling or chemical interaction from the atmosphere in order to create a good bond between the metal contact and the semiconductor. Cleaning methods vary depending on purpose and preference, however common elements are present.

The selected cleaning process consisted of a rinse of TCE, acetone, methanol, and deionized (DI) water, followed by N_2 Dry. The sample was held at the edges by tweezers instead of being held by a spinner due to the small sample size. Rinsing took a period of

10 to 12 seconds per solvent by counting slowly to 12. Care had to be taken when drying with the N_2 gun since the gas velocity was high enough to blow the sample across the hood. One sample was lost in this fashion. The samples were then diamond scribed with their respective positions on the original wafer, and cleaned again. Figure 7 shows the chemicals used in the chemical hood.

Figure 7: Cleaning Supplies in Hood. Samples were cleaned prior to contact deposition

Additionally, the quartz tube used in the tube furnace also required cleaning. Since the material previously used in that tube was unknown, a strong etch had to be performed using the acid aqua regia. Aqua regia, a 3:1 mixture of HCL:HNO_3, is a strong oxidizing agent which gets its name (royal water) from the ability to dissolve the royal metals such as gold and platinum. The etching process ensures that residue left on the tube from previous anneals of different materials does not contaminate current samples. The tube was left filled with acid for about half an hour, when the bubbling from chemical reaction ceased. The tube was then labeled “SiC” to inform future users.

Forming Ohmic Contacts

Ohmic contacts were deposited as soon as all samples were cleaned. Contacts were deposited using the E-beam system depicted in Figure 8. Contacts were placed on the periphery of the samples, as close to the corners as practical. Layers of 150 nm were placed on the samples. Nickel was used for n-type samples, and Al /Ti (70/30) was used for p-type material. Since similar Hall effect studies are being done at AFIT, a suitable contact mask already existed.

Figure 8: E-Beam Deposition System. This system deposited the metal contacts onto the samples

As an initial check of contact deposition, samples were examined by microscope inside of the clean room. Figure 9 is an example of a sample image captured by computer from the microscope. The samples were so large that at the microscope's broadest setting, the entire sample could not be captured. The image collected from each sample corresponds to the worst looking corner.

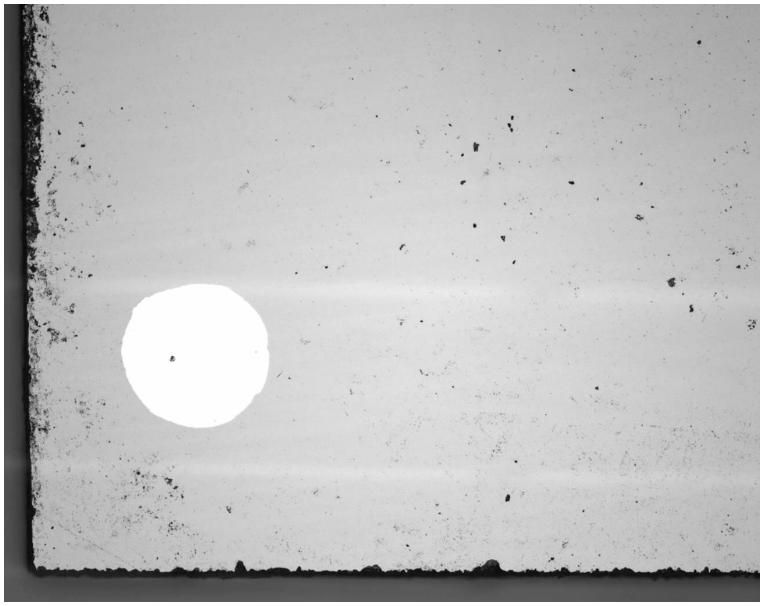

Figure 9: Sample under microscope

After all contacts were deposited on all samples, they were annealed in an annealing furnace. Before samples could be annealed, the quartz tube had to be put through a heating cycle to ensure that any residual moisture was released from the tube since it had just been cleaned.

The annealing procedure was as follows. First, the sample was loaded into the tube, but outside of the furnace. Figure 11 depicts samples in the staging area outside of the furnace. Next, a supply of argon gas was connected to the tube. While nitrogen was originally selected, argon was used during actual annealing because nitrogen is a known

dopant of SiC, and argon is also an inert gas. This had the advantage of inert gas flow without accidentally changing the doping level.

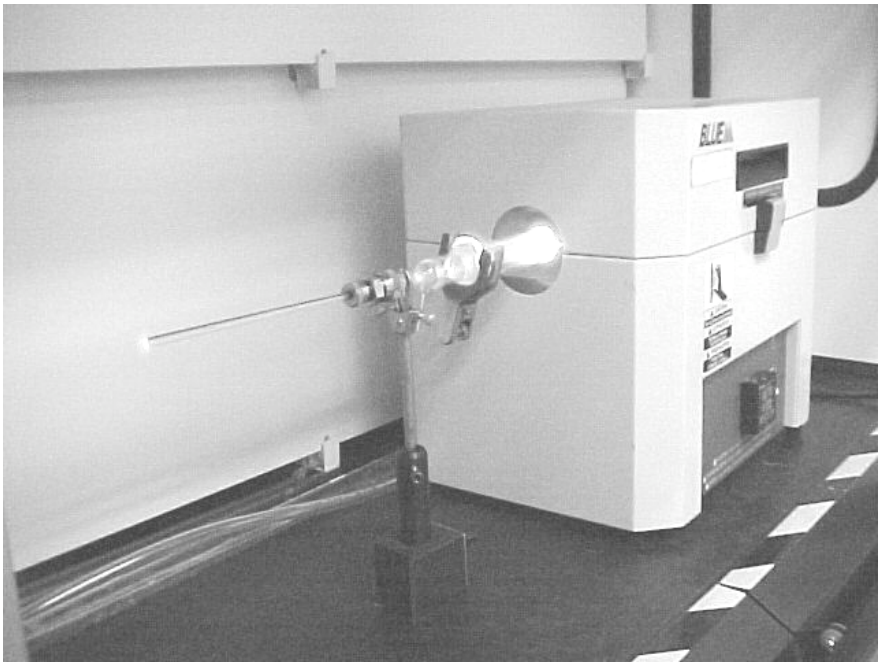

Figure 10: Samples annealing in furnace. Samples were annealed at temperatures of 900° C and1100° C for p-type and n-type respectively.

Once inert gas was flowing, the furnace was turned on. It usually took about 20 minutes for the furnace to reach the set temperature. Once the required temperature was reached, the samples were inserted into the hot furnace for the prescribed period, and then removed to the staging area. N-type samples required an annealing time of 5 minutes at 1100° C, and p-type samples required 2 minutes at 900° C. To prevent oxidation, the samples were allowed to remain under argon gas flow while the samples and the furnace cooled down.

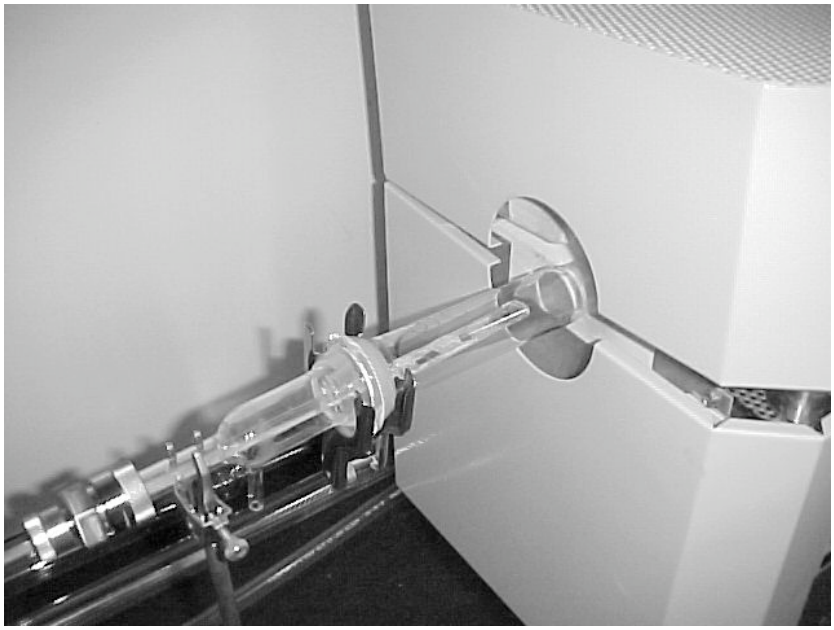

Figure 11 Samples cooling after anneal

The effectiveness of the annealing process was measured using a probe station to take IV data of each sample. Figure 12 shows an image of the probe station used to test the newly formed ohmic contacts. A voltage was applied to contact 1 & 3, measuring the resultant current. The process was repeated with contact 2 & 4 on the sample.

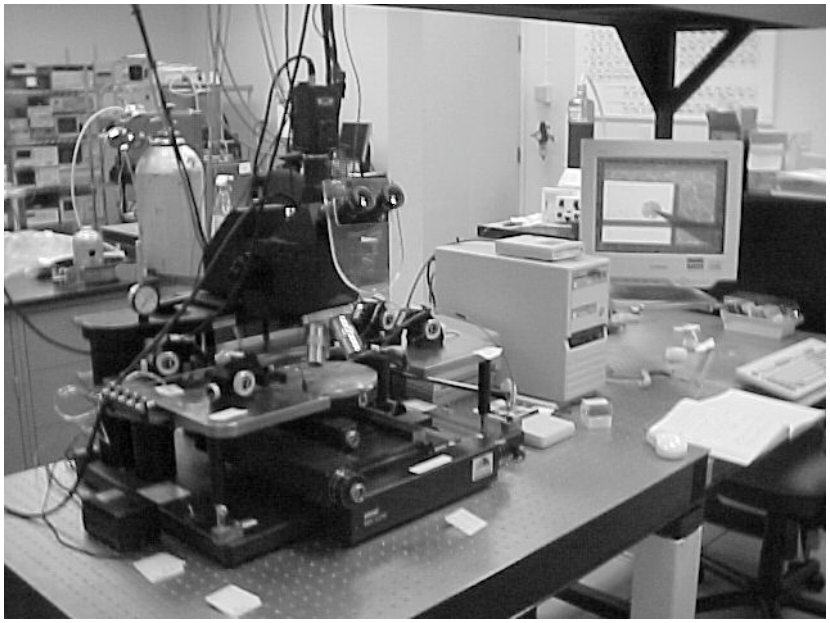

Figure 12: Semi-Conductor Characterization Probe Station. This station was used to take IV measurements.

A properly fabricated contact is one with low resistance ohmic behavior. Most samples displayed the proper ohmic behavior with linear IV plots. An example of the resulting IV curve from a good sample is Figure 13. Figure 14 depicts the result from contacts exhibiting non-ohmic behavior.

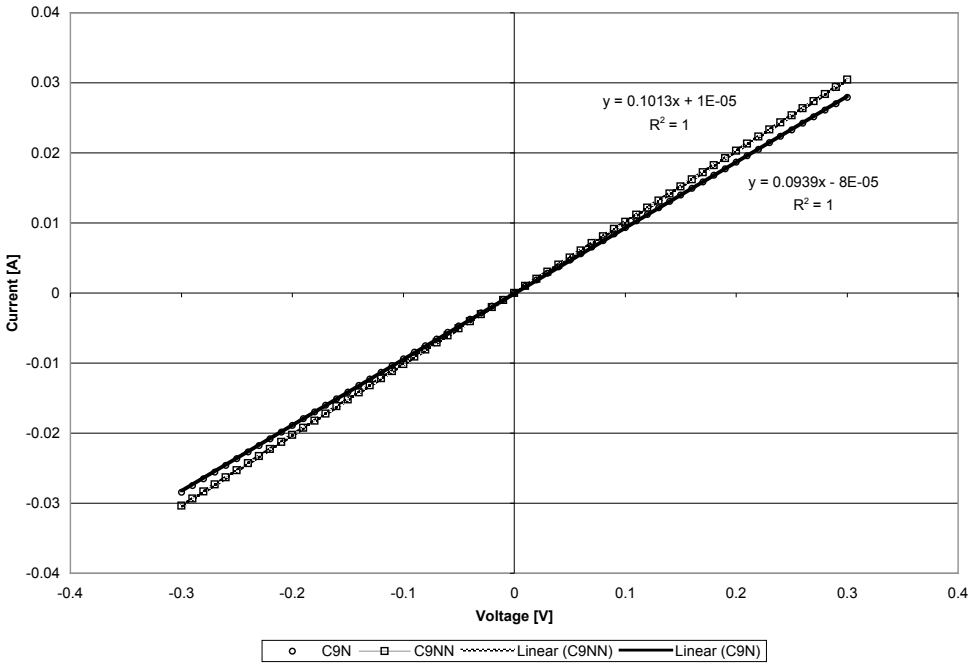

Figure 13: IV curve for n-type sample C9. Note the linear fit.

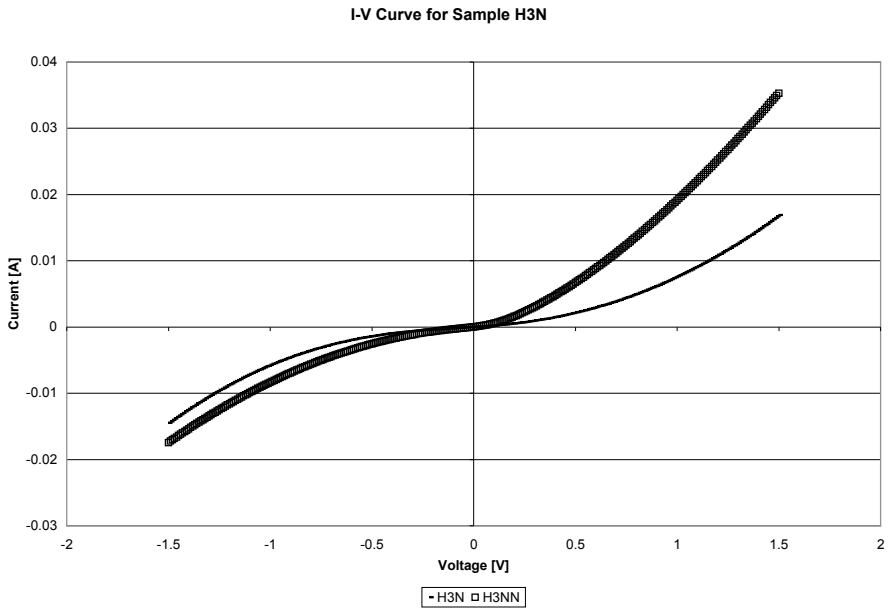

Figure 14: IV curve for n-type sample H3. Note the rectifying behavior.

Wire Bonding

Two methods are common for connecting square Van der Pauw samples to a Hall system. The first method involves using probes to press against the ohmic contacts. The second method is to connect thin wires with a solder, usually indium. The Hall effect system used in this research uses the latter method.

Typically, the Hall wires are soldered to the sample holder. This experiment hinges on minimizing premature heating of the sample, so post irradiation soldering is avoided as much as possible. To avoid soldering wires post irradiation (and inadvertently heating the sample), wires were placed on the samples prior to irradiation. Figure 15 is a picture of a sample with attached wires.

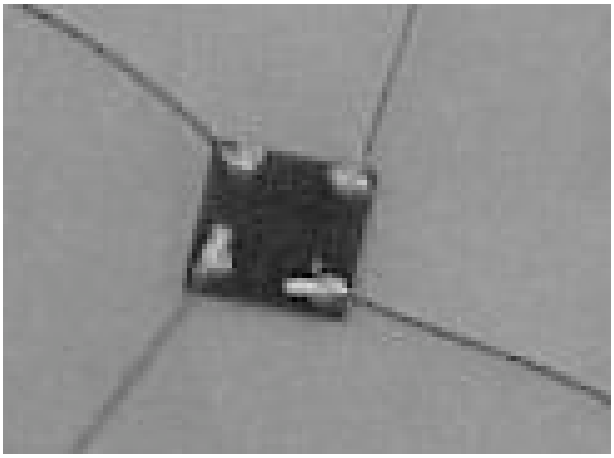

Figure 15: Sample with attached wires

Since pre-irradiation attachment places additional materials in the reactor, connecting wires are required to posses a low, fast spectrum neutron capture cross sections, and survive environments of temperature ranging from 77 K to 500 K.

Common materials used in electronics include gold, indium, silver, aluminum, and copper. Copper and gold were avoided due to activation. Soldering, wire bonding, and conductive epoxy were the three bonding methods available.

I initially settled on wire bonding aluminum wires to the samples. The thin wires used for wire bonding would have had the advantage of low mass, and thus low activation. Furthermore, aluminum is a low-activation material, with acceptable electrical properties. Thus I chose to wire bond aluminum wires to the ohmic pad. This, however presented additional problems with handling since, bonded wires are not usually intended to be handled in the manner proposed, and risked snapping off.

Soldering was then explored. The difficulty with using solder is its generally low melting point. Several high temperature lead / indium solders were located at AFRL.

Unfortunately, none of the solders properly whet the material, not sticking properly to either the nickel or AlTi contacts. Conductive epoxy was the last remaining option.

The conductive epoxy is a liquid containing silver flakes that highly concentrate when cured. A silver / nickel wire was selected to compliment the epoxy.

Since the wires would be irradiated, material selection was important due to activation concerns. To minimize activation, the wires were cut to just long enough to reach the posts on the sample holder. Initial attempts to mount samples on the holder showed that the epoxy connection was fragile. The wires were then bent at right angles to relieve stresses found at the wire / contact junction. Figure 16 shows a sample with shortened bent wires.

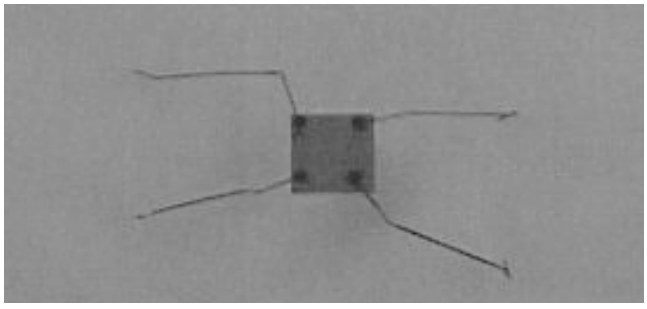

Figure 16: Sample with bent wires in preparation for irradiation.

While this configuration was more resistant to wire detachment, failures still occurred.

Sample Irradiation

Samples of 4H-SiC were exposed to fluences of fast neutrons ranging from 10^{14} to 10^{16} $\frac{n \cdot cm}{cm^3}$ at the Ohio State University's Nuclear Research Reactor (OSUNRR). Corresponding irradiation times are calculated in Appendix B. Due to the high fluence

and required dose, the Central Irradiation Facility (CIF) was used for irradiation. The CIF is a tube that allows access to the center of the reactor. The reactor's rabbit tube was also an option for neutron irradiation, but was not used since the pneumatic tube has a tendency to shock its contents with sudden jolts that may have damaged the wire connection.

In order to ensure low activation, the samples were cadmium shielded. Cadmium is a unique material, allowing most of the fast neutron spectrum to pass through, while filtering most of the thermal neutrons.

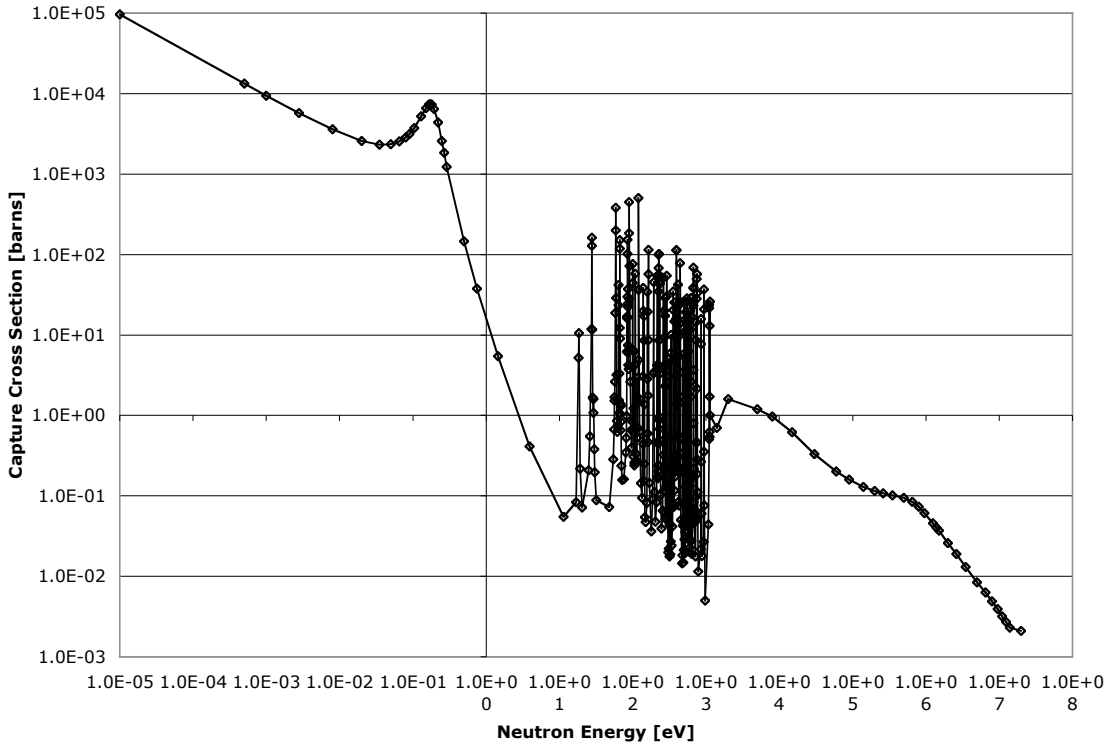

Figure 17: Cadmium neutron absorption cross section as a function of energy. Cadmium has the unique property of a large thermal cross section and a small fast crossection [24]

Since thermal neutrons do not have the energy to create the damage desired in this experiment, using cadmium shielding will not skew results of irradiation.

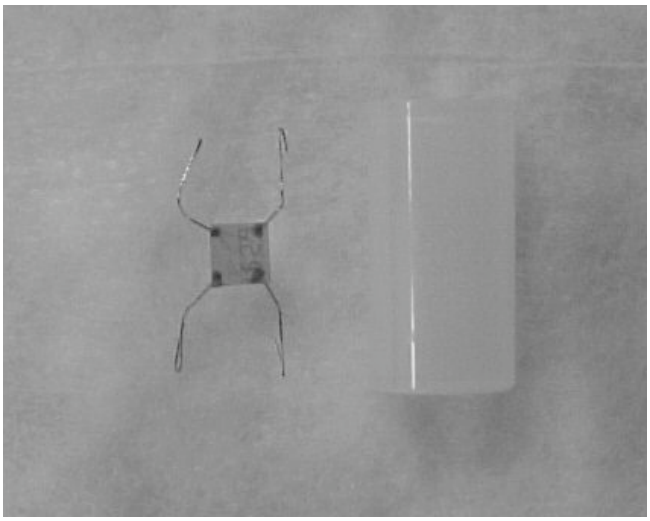

Figure 18: Sample and its Container prior to irradiation.

The SiC devices were placed in plastic containers just big enough to fit the samples. Figure 18 shows the container for a device, while Figure 19 shows a stack of several samples in a run before applying the cadmium wrapping. It should be noted that the amount of cadmium required for 6 samples exceeded allowable amounts of negative reactivity for the reactor. To prevent reactivity problems, only 3 samples were irradiated at a time, reducing the amount of Cd shielding. For higher doses, two samples were placed in one container to further reduce the amount of cadmium required to cover all samples of the run. The required thickness of cadmium can be calculated with (7).

$$I/I_0 = e^{-\Sigma t} \tag{7}$$

leads to,

$$t = \frac{-\ln|0.10|}{\Sigma} \approx \frac{2.250}{\Sigma}$$

where, I/I_0 ~ intensity,

Σ ~ macroscopic crossection, and

t ~ thickness.

Using Σ=463 (1/cm), and 90% thermal neutrons filtered, t = 0.005 cm or 2 mil.

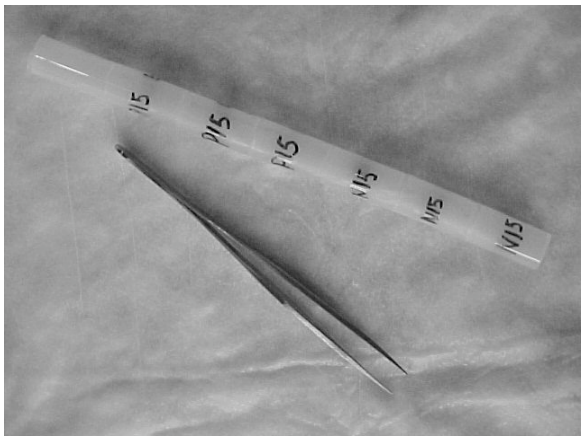

Figure 19: Samples to be irradiated

While the cadmium wrapping prevented activation, a disadvantage of the cadmium became apparent. The cadmium acted as a poison, a neutron absorbing substance adding negative reactivity. To counteract the poison, control rods were withdrawn. For safety reasons, control rod withdrawal is limited. Due to additional negative reactivity, the number of samples stacked were reduced from 6 to 3 in order to reduce required cadmium shielding. For future experiments, it is suggested to combine samples together in a small space to reduce the cadmium requirement. Additionally, using the minimum thickness of cadmium required would reduce negative reactivity.

Figure 20: Containers wrapped in cadmium. Cadmium's high thermal neutron cross section helps to minimize activation of the samples.

Measurement Procedure

Once the system was operational, a method had to be devised to mount the samples to the cold head. The nature of this experiment requires the sample to stay as cold as possible during mounting, eliminating use of solders, which would add heat through the wires. Additionally, the junction between the wire and the ohmic contact, which was held by silver epoxy proved to be very fragile.

Several mounting techniques were attempted without satisfactory results. These techniques included using conductive epoxies, solders, and attaching thinner wires. The method finally implemented, required removing the pre-connected wires, and connecting a new wire (which is soldered onto the sample mount) to the sample using a conductive silver epoxy. Since curing the epoxy was not an option after irradiation, a dab of rubber cement was placed on the wire to hold it in place. Using an uncured epoxy added minimal resistance to the contacts.

After ohmic contacts had been applied to the surface of the SiC, the initial mobility of the samples needed to be recorded. The same process was followed for the Hall effect measurements before and after irradiation.

Samples were characterized after device fabrication and irradiation. Three samples per type were reserved for initial characterization, corresponding to a neutron fluence of zero. The remaining 12 samples were irradiated at OSUNRR facility as described in the irradiation section.

In order to characterize from 100K to 340K, the unirradiated samples must first be cooled with liquid nitrogen. Irradiated samples are cooled in liquid nitrogen to damage since vacancy and interstitial damage are immobile at temperatures less than 80 K [17:82].

Samples were bonded to the sample mount using rubber cement. The wires on the sample were then soldered onto the pins of the sample mount. Finally, the sample mount was replaced into the cold head.

Hall measurements over a temperature range from 100K to 340K at 10K increments were measured. The lower end was decided due to limitations on keeping the device at liquid nitrogen temperature during mounting, accepting a 23K buffer above 77 K as reasonable. The upper limit temperature was limited by the bounds of the Hall effect system. Measurements reaching temperatures of 500K were desired, but a system capable of both low and high temperature measurements was not available.

Hall Effect measurements are widely used, and Standard F76 is published by ASTM to ensure continuity. However, a copy of the standard was not purchased for this

study. NIST has a recommended procedure published on there website, and Runyan makes additional recommendations, both based on ASTM F76 Standard [41, 51]. A detailed description of how to take Hall Effect measurements can be found in Appendix A

IV. Results

The results of this experiment are broken down into two sections. First, the S110 was unable to match parameter values of the unirradiated characterization samples with AFRL's Hall system. Characterization data is compared and differences between systems is identified to narrow down the problem, but no particular feature is identified as the cause. Second, results pertaining to irradiated samples are reported. No features seen in the data suggest annealing behavior below a temperature of 350K. Characteristics expected from neutron damage are identified. An anomalous spike in values is seen on occasion at temperatures of about 280K, and explained as a result of using an uncured epoxy on some samples.

The following data was collected from n-type samples irradiated with 10^{15} and 10^{16} $\frac{n \cdot cm}{cm^3}$, 1 MeV equivalent fluences, along with an unirradiated set of samples. P-type samples, and n-type samples irradiated to 10^{14} $\frac{n \cdot cm}{cm^3}$ were not measured due to time restrictions.

Additionally, the temperature range of interest was restricted due to equipment limitations. The AFRL Hall system had a ceiling of 340K, while the S110 system had a ceiling of 425K. Initially, a temperature of 500 K was the goal of the experiment, but measurements could only be recorded up to each system's respective limit.

A few samples were eliminated due to the inability to form ohmic contacts. Fifteen out of twenty contacts of each type developed sufficient contacts. The n-type samples selected had contact resistances ranging from 10 Ω to 40 Ω, which lead to

resistivities on the order of $10^{-5}\ \Omega - cm$. The literature states that good ohmic contacts should have resistivities on the order of $10^{-5}\ \Omega - cm$. P-type samples had resistances from 90 Ω to 200 Ω, but were not measured.

Sample population decreased further after wire contact formation. Due to the combination of stiff wire and a brittle connection to the ohmic contact, the silver epoxy often separated from the contact. Samples broken prior to irradiation were removed from the pool of samples.

S110 & Characterization Measurements

The first objective of this experiment was to set up and characterize a Keithley S110 Hall effect system. Temperature dependent Hall measurements of unirradiated samples were taken using AFRL/SN's Hall system to compare to the results from the S110 system.

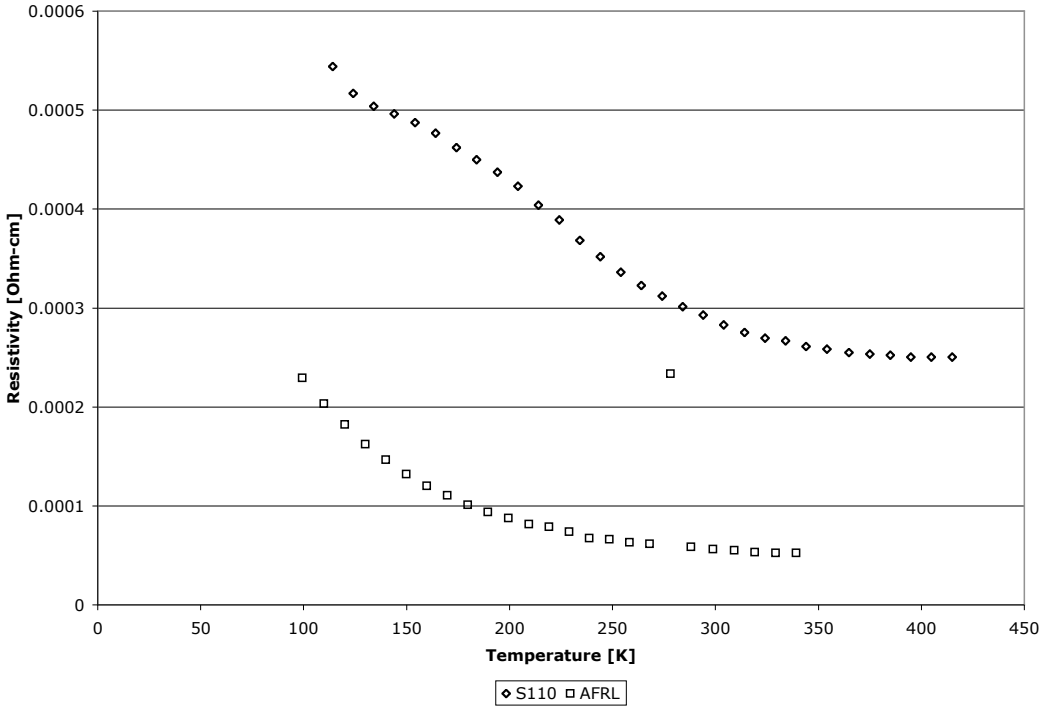

Figure 21: Comparison of Resistivity Measurements between S110 Hall System and AFRL's Hall System

Measurements of resistivity from the S110 were much greater than those taken by AFRL as depicted by Figure 21. This result is surprising because the most significant difference between the two systems was with the connection of the sample wires which can be accounted for in the calculations. The S110 samples had a cured silver epoxy connection, while an uncured silver epoxy was used on the AFRL system. Since the cured sample has an increased density of the silver flake in the epoxy, it is reasonable to expect the cured sample to result in a lower resistance. Studies with irradiated samples, discussed in the next section, composed of both cured and uncured contacts show no difference in resistivity results.

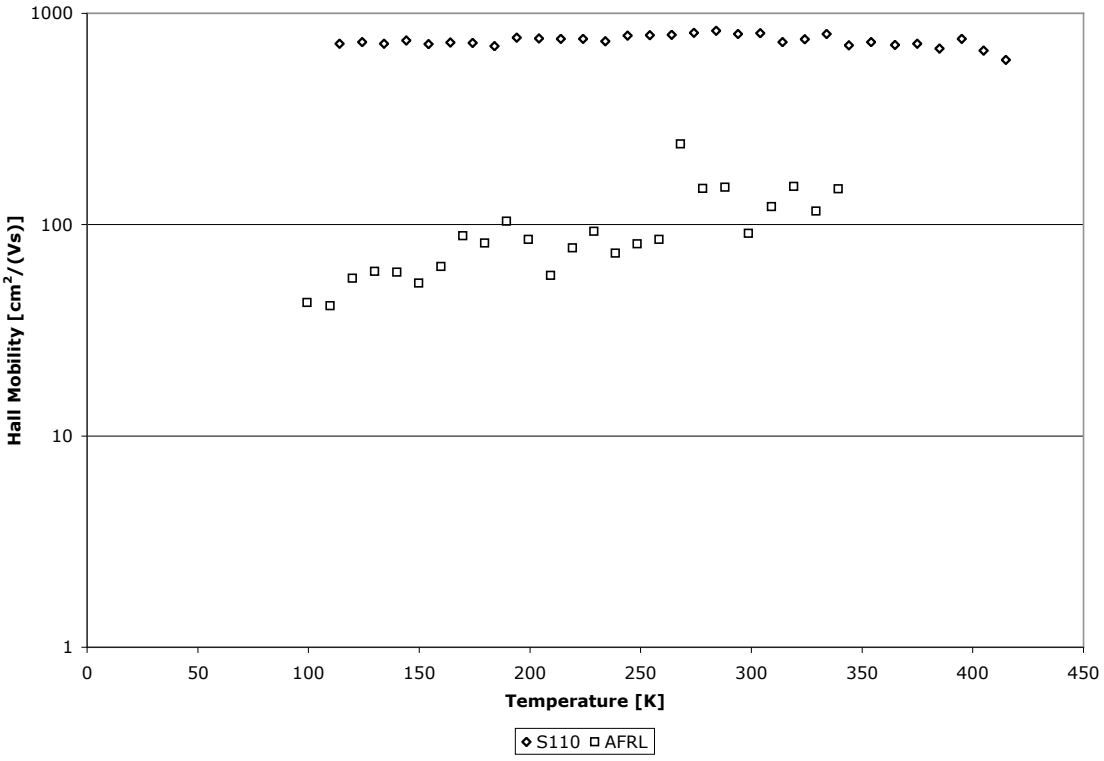

Figure 22: Comparison of Hall Mobility between S110 and AFRL Hall systems

Figure 22 presents the results of Hall mobility for both systems, and is calculated from the results of the Van der Pauw resistivity and carrier concentration measurements. In general, mobility increases with temperature at similar rates for both systems. The figure indicates a higher mobility for the S110 measurements than those measured at AFRL. Mobility values are characterized on the order of 10^2 [cm^2/(Vs)] using the AFRL system.

Figure 23 depicts the mobility results from the S110 system alone. The literature reports a maximum in mobility just below room temperature. Figure 23 shows a local maximum at 280K which is difficult to discern due to the high variance in the mobility values. This peak mobility has an average value of 826 cm^2/(Vs). This peak is not

obvious from the results taken at AFRL. A second order polynomial fit is shown as a rough approximation to emphasize the general trend. It is not a good fit since the maximum is a result of a changeover in driver from impurity scattering to acoustic phonon deformation scattering [22].

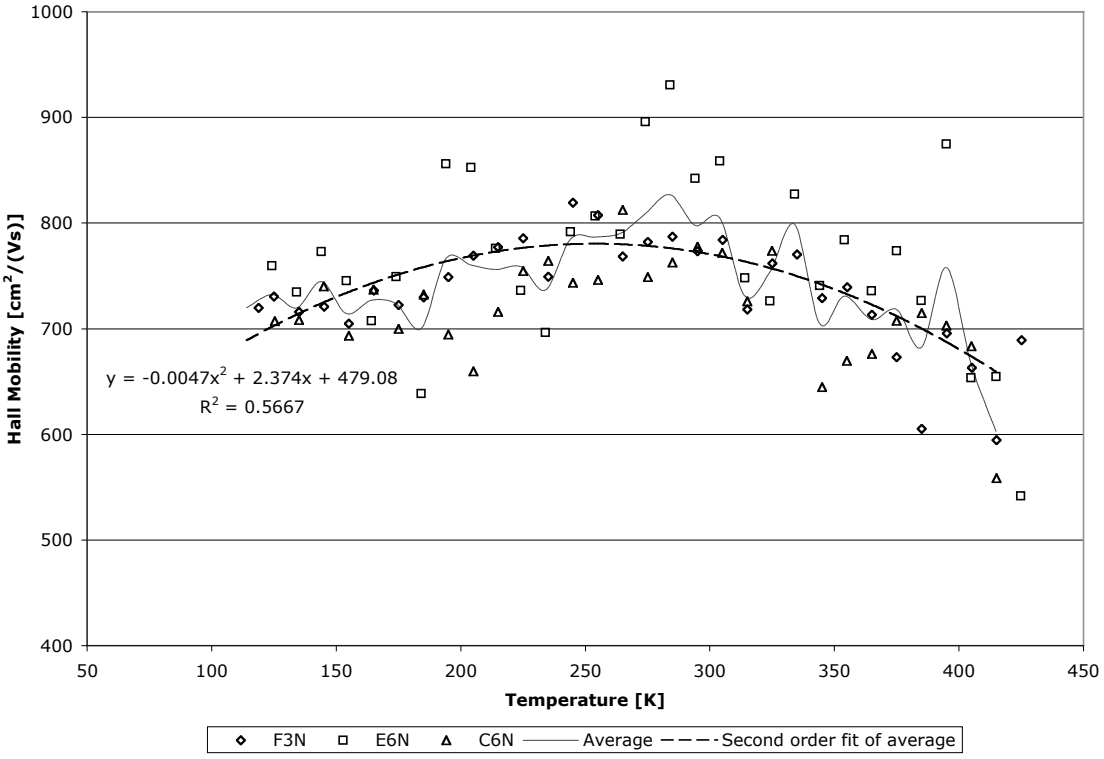

Figure 23: Characterization of Hall Mobility using S110 Hall Effect System

Bulk carrier concentration as measured by the two systems also greatly varies. Figure 24 suggests a linear increase in carrier concentration with temperature as measured by the S110 system. Theory models the temperature dependence of carrier concentration as an exponential.

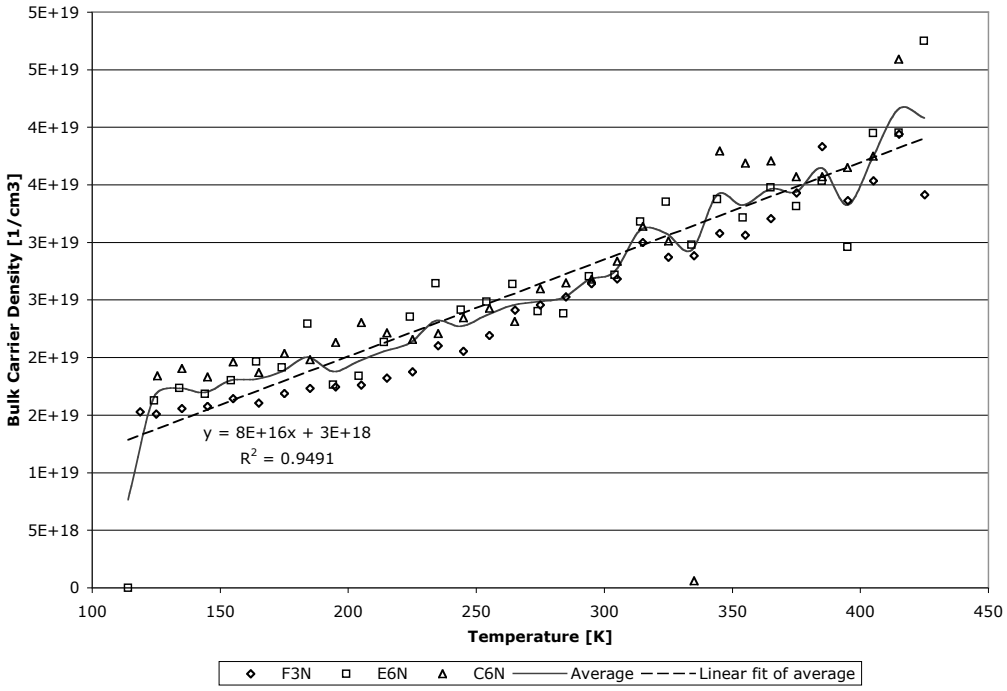

Figure 24: Bulk Carrier Concentration of 4H-SiC using S110 Hall System

Figure 25 shows much greater bulk carrier concentration from the AFRL system than with the S110 system. The difference in values may be a result of the difference in magnetic fields used between the two systems. The variance in carrier concentration carries over into the mobility calculation and increases with temperature due to thermal noise. Increasing the current flow, discussed in the next section, dramatically decreased the amount of variance by adding carriers thus increasing Hall voltage.

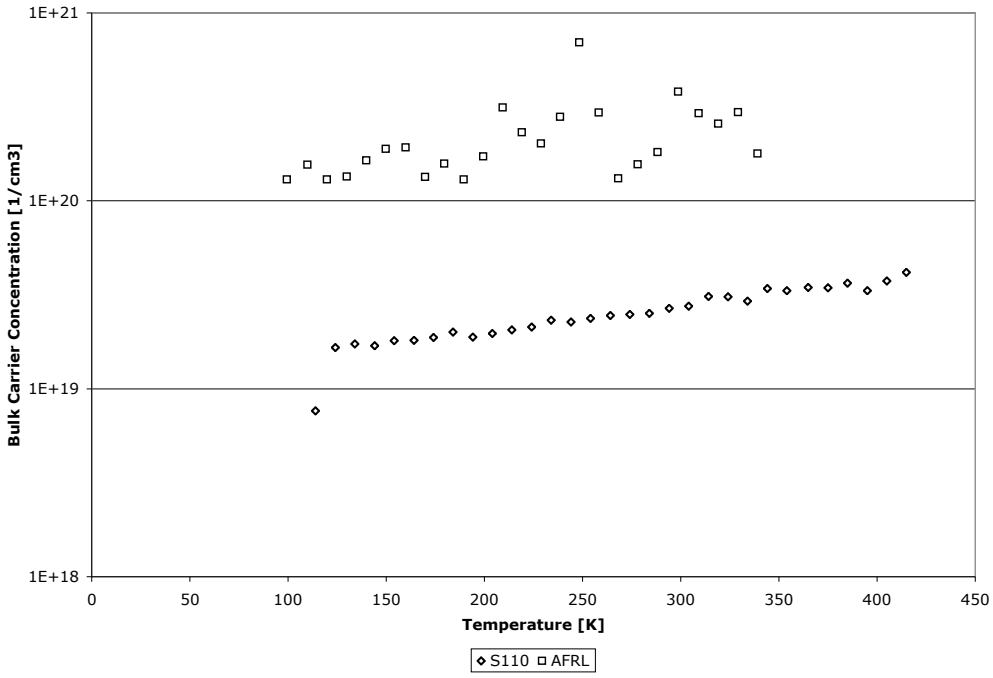

Figure 25: Comparison of Bulk carrier concentration between S110 and AFRL systems

As a tool to troubleshoot the program for S110, a visual basic program was written to take measured currents and voltages, and calculate resistivity, mobility, and carrier density using the same routines that the S110's program used. Using the measurements taken at AFRL, I confirmed that the program correctly calculated the desired parameters. Figure 26 is a depiction of the program confirming AFRL's results from the measurements.

By ruling out an error in calculation, the source of the discrepancy can be narrowed down to either an error in taking a measurement, or a difference in a system parameter, such as magnetic field strength. In the process of setting up the equipment, each instrument was checked many times against a known load. Additionally, delays were programmed into the code to allow a device to settle before requesting data to ensure proper measurement. Therefore, I suspect that the difference in results comes from

a difference in system operation. Differences were noted in the quality of the wire connection to the sample, the strength of the magnetic field, and the medium filling the cold head.

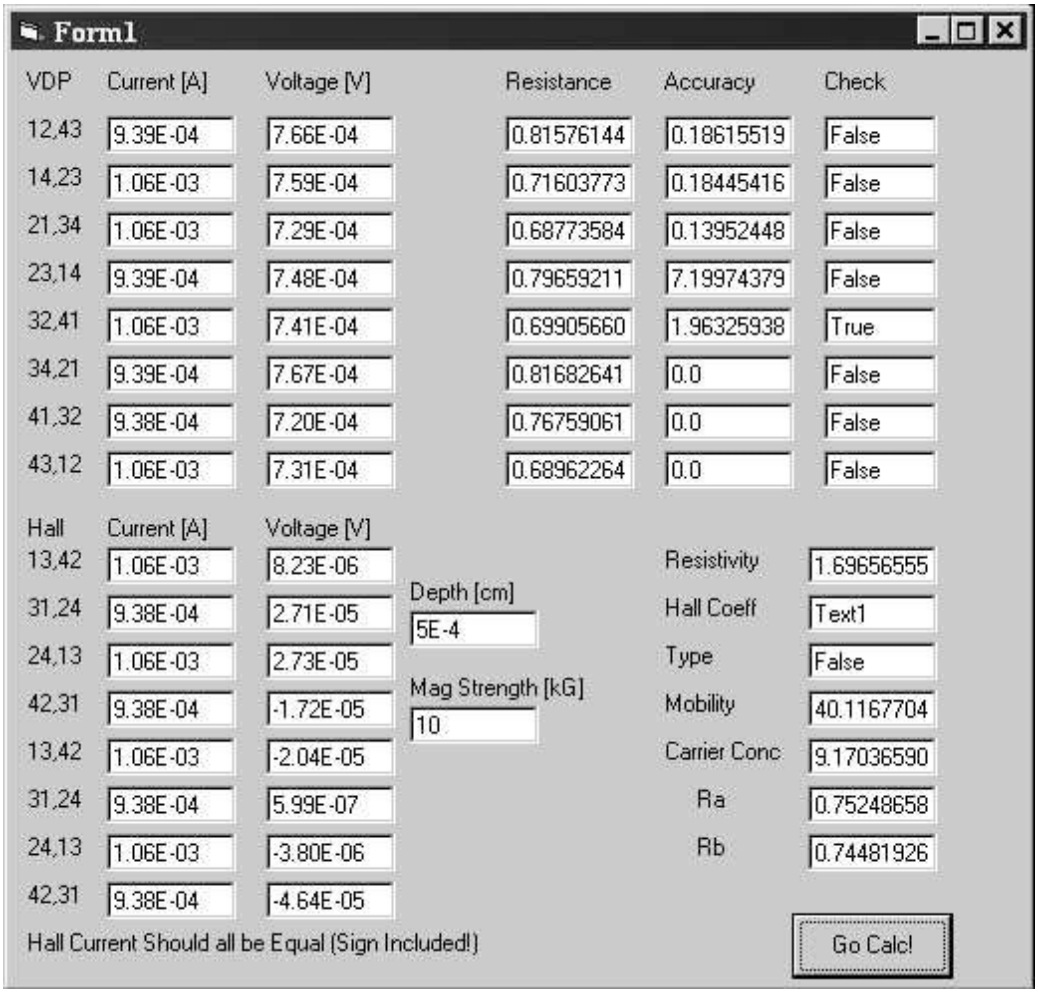

Figure 26: Interface for Hall effect calculation program.

For the S110, each sample had the original wire with the cured epoxy per the original plan. Through mounting, unmounting, and handling, many of the fragile wire connections broke. At AFRL, an uncured silver epoxy was applied to the exposed ohmic contact to make the connection. The resistance of the cured samples, as measured on a digital multimeter, was ~10 Ohms while the uncured samples were ~50-100 ohms. While

the uncured epoxy had a slightly higher resistance, it wasn't enough to cause the observed differences.

The difference in magnetic field is also unlikely to have played a significant role. I was unable to get the S110's magnet above 1kG, and operated it at 0.7 kG. AFRL operated at 10 kG. Since the magnetic field operates during the Hall measurement, and not the Van der Pauw measurement, it would only effect the measured Hall voltage, and not the resistivity. Likewise, the calculation of carrier concentration from the Hall voltage already includes the strength of the magnetic field, so even with different fields, the average value should not differ as much as observed between the two systems. A stronger magnetic field, however, more effectively separates the charge carriers, increasing Hall voltage, and decreasing variance.

The S110 system evacuated the cold head before cooling to prevent problems from moisture freezing. The AFRL system employs a stream of liquid hydrogen to displace the air and have a similar effect. The advantage of a streaming gas is the reduction in cooling time, thus increasing the sampling rate. It is unlikely that this difference had any effect on the system as well, but is mentioned for completeness.

Unfortunately, this qualitative discussion does not quantitatively address the accuracy of the S110 system. To better troubleshoot the S110 Hall effect system, a standard sample should be used. In place of a calibrated standard, a device similar to the ones fabricated in this thesis made of silicon could be used, since the electrical properties of silicon are better understood than SiC.

Radiation Effects

In order to assess the effects of neutron damage, it was required that samples be mounted quickly to minimize warming. The S110 did not allow for quick sample cooling, so measurement of the irradiated samples also took place at the AFRL sensors directorate. The S110 took 3 hours to cool the sample to 100 K, while the AFRL system had the sample back to 100 K in 30 minutes, in addition to the mounting time. The characteristics of concern are resistivity, Hall mobility, and carrier concentration. Since all of the irradiated samples were measured using AFRL's equipment, the AFRL characterization data discussed in the previous section is used for comparison.

Irradiated samples show increased resistivity from the unirradiated samples. The average results, depicted in Figure 27, suggest that resistivity for the two sets of irradiated samples differ from the characterization set by a multiplication factor in agreement with theory. Theory states that the resistivity of an irradiated sample will be the resistivity of the unirradiated sample times a quantity determined by the neutron fluence received [37:242]. Resistivity in all samples appear to decrease as $T^{-1.2}$. However, a difference between the resistivity of the two irradiated sets is not obvious due to variance. The lowest resistivity achieved was 5.01E-5 Ω-cm occurring at 330K, supporting the claim that good n-type ohmic contacts formed.

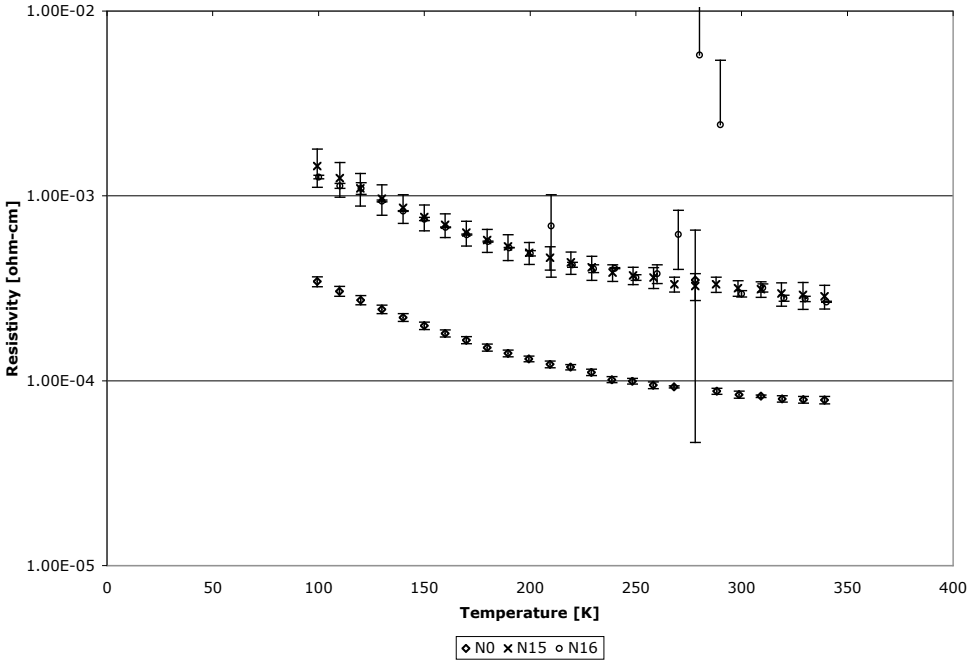

Figure 27: Average Resistivites of n-type samples by neutron fluence received

Up to 340K, the decrease in resistivity with temperature was expected. Above this temperature, resistivity is expected to increase as phonon scattering becomes dominant over Coulombic scattering from impurities and thermal excitation of carriers into the conduction band.

Note that an anomalous point occurs at 278K, just above the melting point of water at 273K. This effect was only observed with samples measured at AFRL, so it is not likely particular to the material. Also, it was observed with irradiated and non-irradiated samples alike, so it is not an artifact of irradiation. A likely explanation is that water is a component of the paste being used, and changed the resistance of the contact as it melted and settled.

It is important to note that sample D6N was not included in the average of irradiated samples. Sample D6N was irradiated with a fluence of 10^{16} 1-MeV equivalent

neutrons, but did not show any signs of damage. The resistivity of D6N in Figure 28 is very similar to the average resistivity of the non-irradiated samples shown in Figure 27. For this reason, D6N was not included in the average of the 10^{16} fluence group.

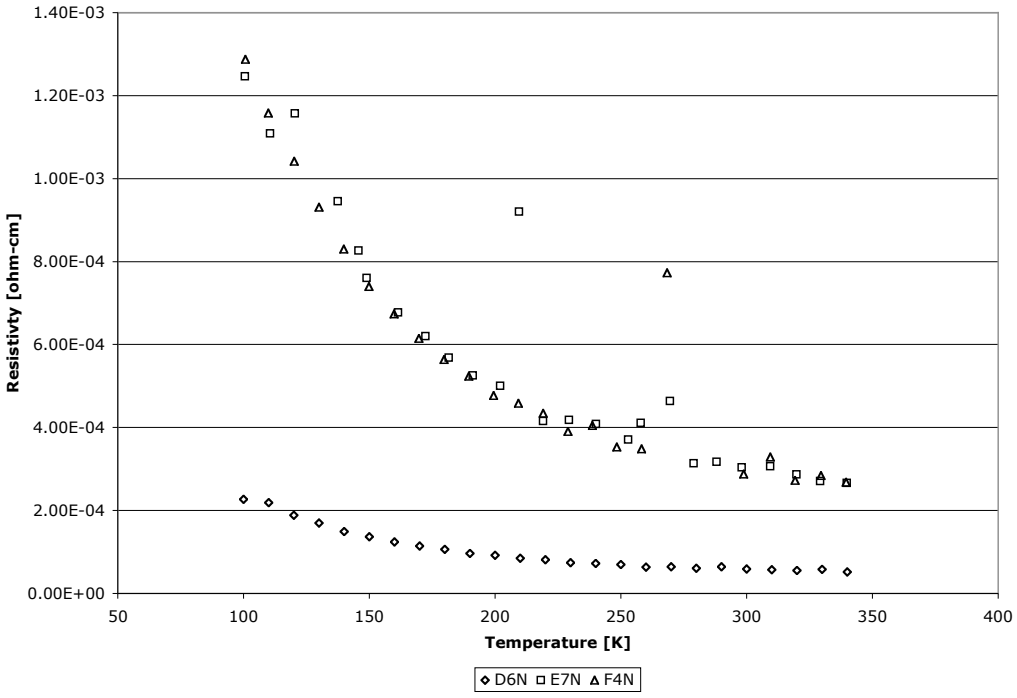

Figure 28: Resistivities of 4H-SiC samples irradiated with 10^{16} 1MeV equivalent neutrons

Carrier density decreases with irradiation due to the creation of active acceptor defects within the band gap. These defects rob the conduction band of carriers, decreasing carrier density. The defect is formed when dislocated silicon or carbon atoms chemically bond with an impurity, such as a dopant, within the lattice [37:197]. Figure 29 shows almost an order of magnitude decrease in carrier density to irradiated samples. Once again, the difference in effect between the two fluences is small. Carrier concentrations were on the order of 10^{20} $\frac{carriers}{cm^3}$ for irradiated samples.

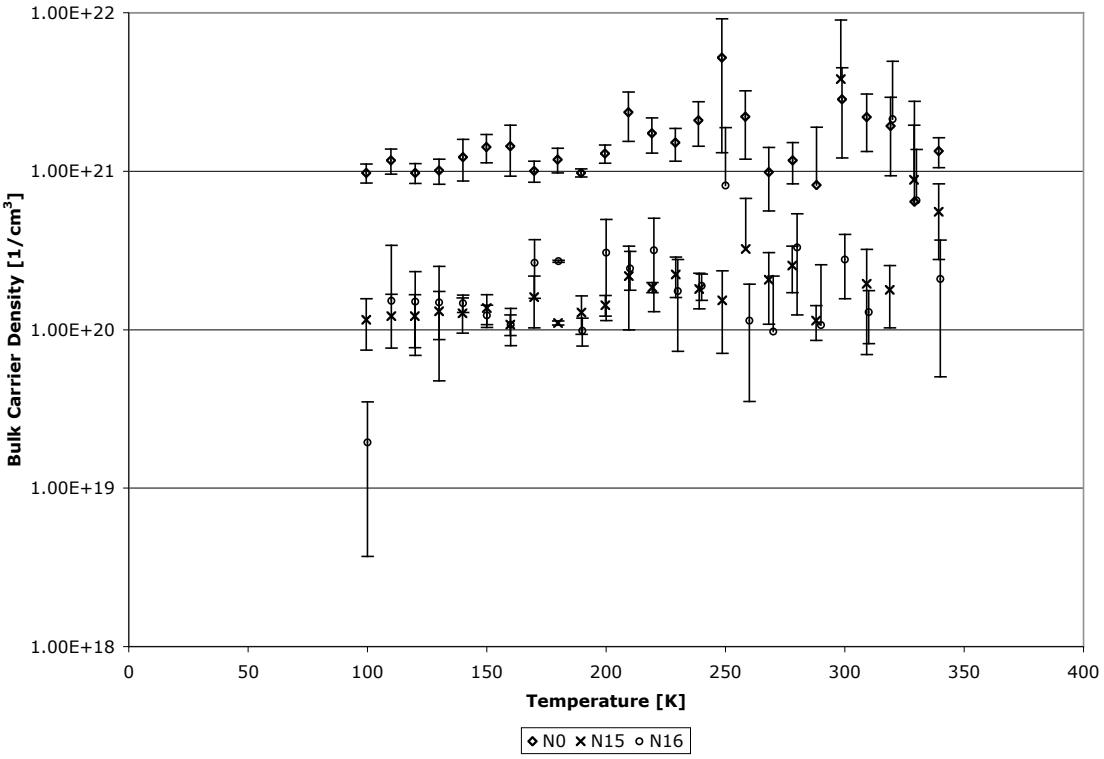

Figure 29: Average Bulk Carrier Density for n-type 4H-SiC by neutron irradiation

The order of magnitude (10^{20}-10^{21} cm^{-3}) of the bulk carrier density compared to the dopant concentration of ~10^{17} cm^{-3} suggests that the measured value is high. The likely source of error is rooted in the assumption that current is isolated to the upper most 5 μm epilayer. The n-type samples contained an n-type buffer region 10^{18} in concentration and 0.5 μm in depth. If the current is penetrating further into the substrate layer, then the extra depth of 400 μm can significantly alter the carrier concentration calculation. The doping level of the substrate is unknown, but estimated to be ~10^{15}.

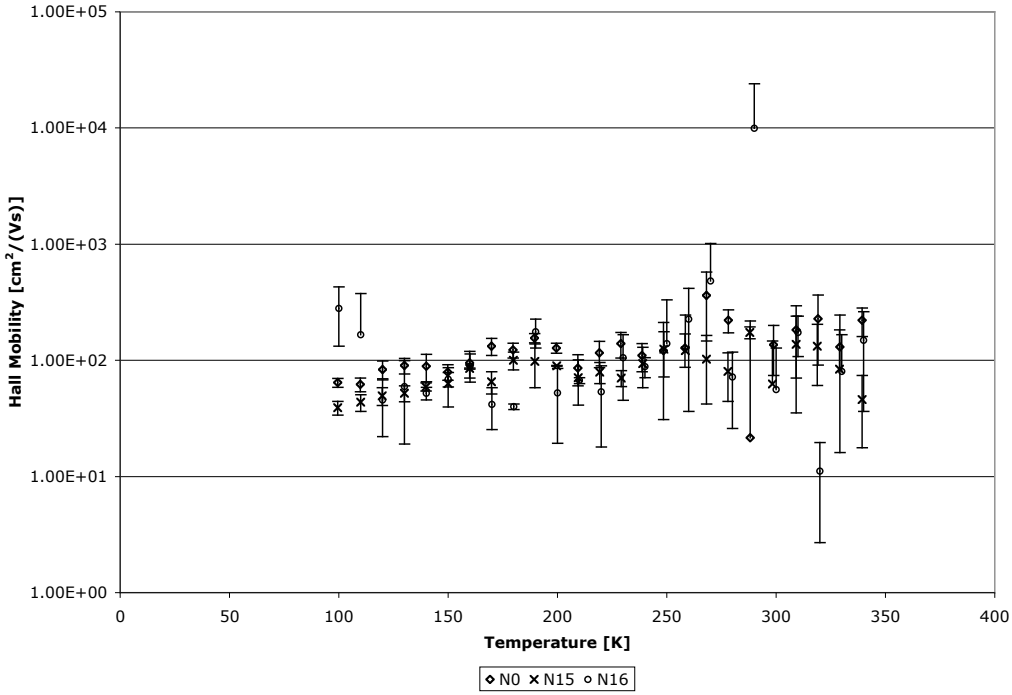

Figure 30: Average Hall Mobility of n-type 4H-SiC separated by neutron fluence

A decrease in mobility with irradiation was expected. However, Figure 30 shows that the difference in mobilities between irradiated and non-irradiated sets are too small to be quantified, since most of the samples lie within a standard deviation of each other. This suggests that neutron damage effects carrier concentration more than mobility.

The largest difficulty in analyzing the data from this experiment has been due to the large variance found in carrier concentration. It was found that increasing the sourced current reduces variance. Sample E9N was run first with a 1mA source, and again with a 10mA source. The results from the second case show much reduced variance up to a temperature of 200K, where thermal noise becomes apparent. This improvement is critical to identifying features in the data.

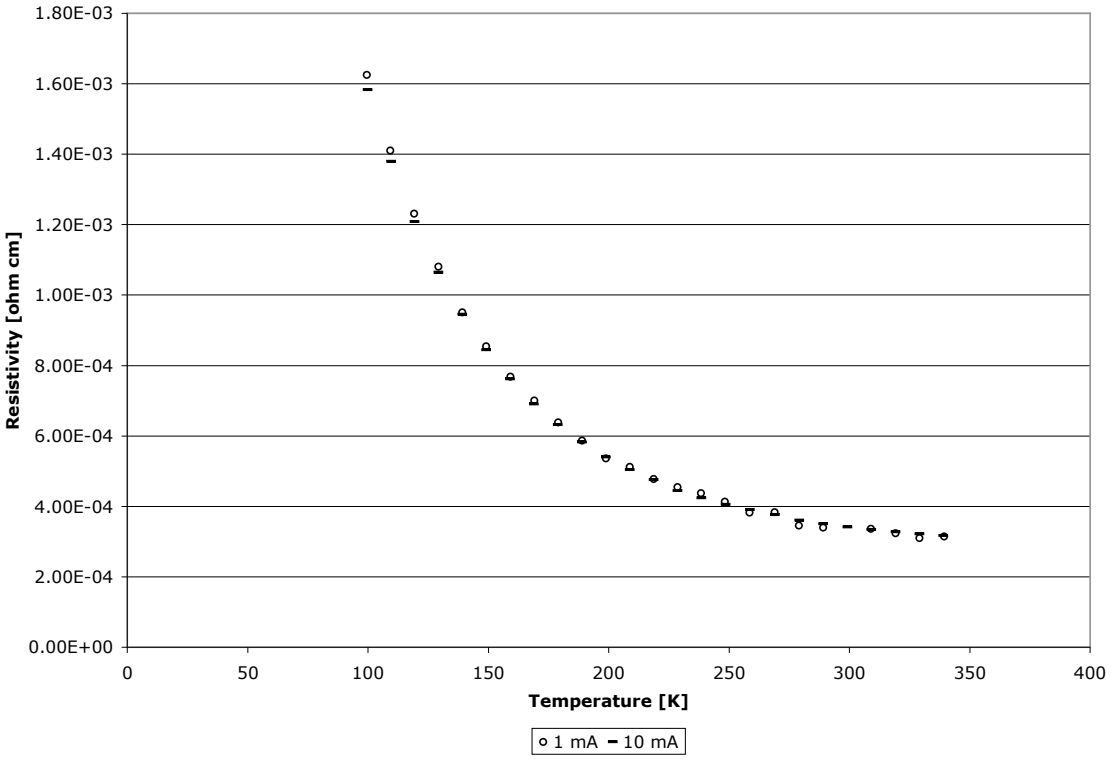

Figure 31: Resistivity of Sample E9N. The first run used a 1mA source current. The second run used 10mA.

Figure 31 shows that the increased current had little effect on resistivity. The benefit is strongly coupled to measurements and calculations dependent on Hall voltages. Figure 32 shows features in carrier concentration that were not previously visible due to large variance. A minimum carrier concentration is identified at 130K.

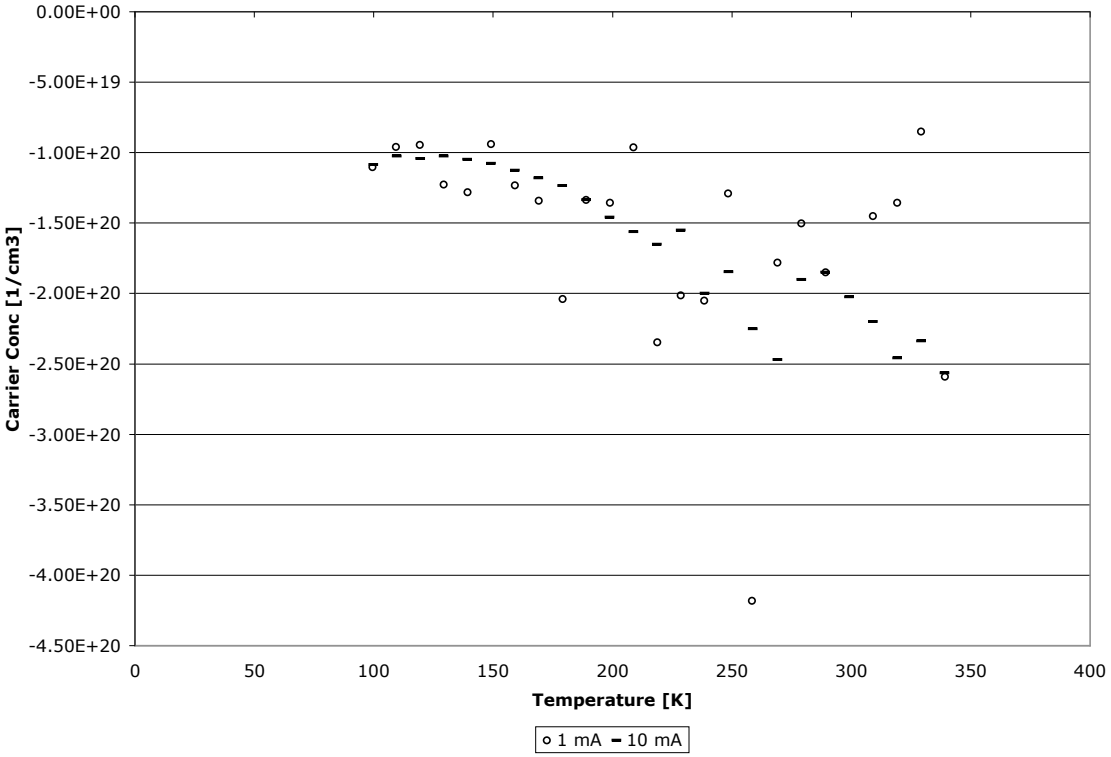

Figure 32: Carrier concentration of sample E9N. The first run used a 1mA source current. The second run used 10mA.

Due to the improved variance on carrier concentration, the variance on mobility also decreases. Figure 33 shows features in mobility not visible in previous runs. A maximum mobility appears at 290K, similar to the supposed maximum described in the S110 section.

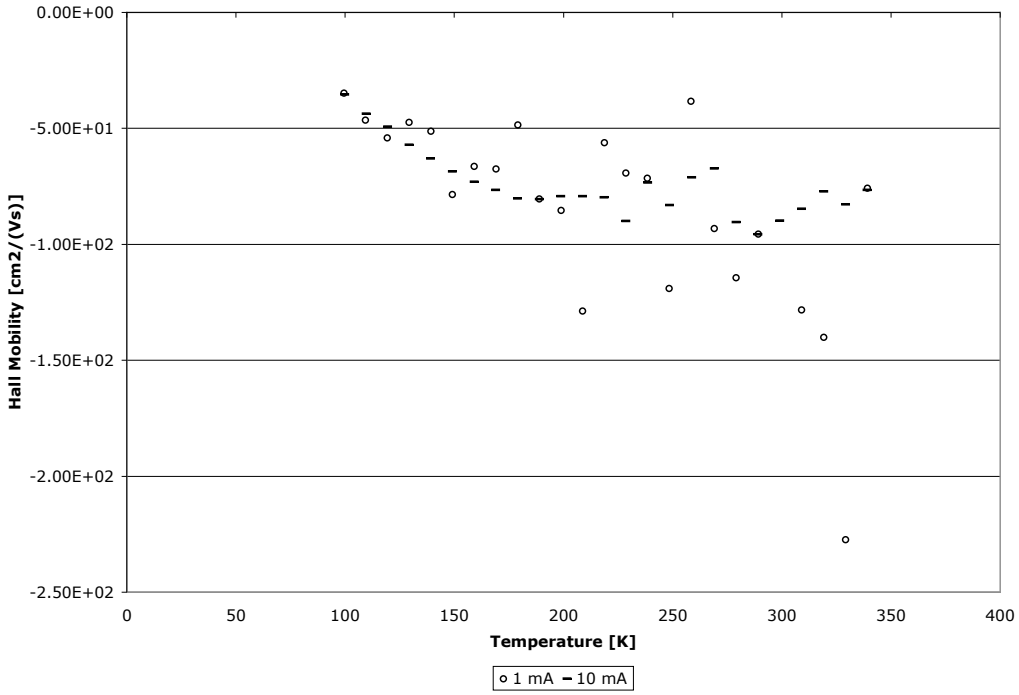

Figure 33: Hall mobility of sample E9N. The first run used a 1mA source current. The second run used 10mA.

Since the increased current test was only performed on one sample, the variance cannot be calculated. It is apparent however, that choosing a proper source current is very important to accurately measuring a Hall voltage.

V. Conclusions

Concluding Remarks

This study attempted to identify low-temperature annealing of neutron irradiated 4H-SiC. No features suggesting annealing below 340K were witnessed in this study. It was determined that a proper source current is vital to identifying features that may become hidden in the variance. Since studies conflict on whether damage occurs at temperatures below 473K, there still may be annealing points between 340K and 500K. This annealing may be limited to the surface as is the case with traditional silicon.

In support of the objective, a Hall effect system was set up. The S110 system set up in support of this study was found to be inadequate due to a long cooling time. Specific problems included a 3 hour cool down time, providing samples with too much time to warm, and possibly removing damage through annealing. Additionally, a probe based sample holder would be beneficial for this type of experiment so that wire connections could be avoided, thus reducing activation and annealing during mounting.

Silicon carbide samples were irradiated and characterized. A separate set of characterization data was collected from both the in-house S110 system and the AFRL based system. The scaling of each result differed although general trends appeared similar. The reason for the different values may lie with the different methods of wire connection, in combination with the use of a much stronger magnetic field at AFRL. The use of pastes in place of solders is not recommended since some components may freeze

and melt during measurement. Table 4 reviews average room temperature (300K) measurements measured using both systems.

Table 4: Summary of Characteristics as measured by the S110 and AFRL at 300K

Characteristic	*S110*	*AFRL*
Resistivity [ohm-cm]	2.80E-04	5.60E-05
Hall Mobility [cm^2/(Vs)]	804	91.1
Bulk Carrier Conc. [1/cm^3]	2.70E+19	3.80E+20

Suggested Studies

A repetition of this experiment is merited since measurements between room temperature and 500K may still prove to show surface annealing. The following suggestions may then be helpful:

- Use a probe station to connect samples. Many of the problems in this experiment stem from the decision to pre-attach wires to the samples. Wires mean more material to be activated, and must be carefully chosen. Additionally, a fragile wire and/or wire connection to the contacts can break rendering an otherwise good sample useless. No wires mean a smaller package to be irradiated, and less cadmium required to shield, which is important if the sample effects reactivity in the reactor.
- Allow ample time for each measurement. Measurements for this experiment took about 8 hours to complete. At a rate of a sample a day, 30 samples would take at least a month.
- Find a system that is able to complete both low and high temperature measurements. Many systems only conduct high or low temperature measurements.

Glossary of Abbreviations

AFIT	Air Force Institute of Technology
AFRL	Air Force Research Lab
CIF	Central Irradiation Facility
DI	Deionized
MOS	Metal Oxide Semiconductor
NTD	Neutron Transmutation Doping
OSUNRR	Ohio State University Nuclear Research Reactor
PKA	Primary Knock-on Atom
SiC	Silicon carbide
USAF	United States Air Force

Appendix A: Hall Effect Procedure

NIST posted the following recommended procedures based on ASTM F76 as a starting point for beginning Hall Effect measurements. [41]

Hall Effect measurements using the Van der Pauw method requires an arbitrarily shaped sample with four contact on the periphery as far apart as possible. A cloverleaf geometry is preferred to minimize error, but sample can also have a square shape.

The following procedures correct for possible electrical non-symmetry from non-symmetric contact placement by taking two sets of measurements, reversing the magnetic field between sets.

Part A) Van der Pauw measurements without Magnetic Field

1) Setup current through sample with power less than 5 mW (pref 1 mW)
2) Apply current I_{21} and measure V_{34}.
   Note: I_{21} refers to the current entering contact 2 and leaving contact 1.
   V_{34} refers to the voltage across contacts 3 & 4.
3) Reverse the current applying I_{12} and measuring V_{43}.
4) Repeat steps 2 & 3 to measure V_{41}, V_{14}, V_{12}, V_{21}, V_{23}, V_{32}
5) Calculate the Resistance for each I, V data pair using ohm's law.

Accuracy Check: The following relations should be correct to within 5%

Note: $R_{21,34} = \frac{V_{34}}{I_{21}}$

$R_{21,34} = R_{12,43}$ $\quad$ $R_{43,12} = R_{34,21}$

$R_{32,41} = R_{23,14}$ $\quad$ $R_{14,23} = R_{41,32}$

$R_{21,34} + R_{12,43} = R_{43,12} + R_{34,21}$

$R_{32,41} + R_{23,14} = R_{14,23} + R_{41,32}$

If accuracy check fails, check system for possible sources of error.

Part B) Hall Measurements with Magnetic Field

Note: V_{24P} refers to voltage measured in a positive magnetic field and V_{24N} refers to voltage measured in a negative magnetic field.

1) Apply a positive Magnetic Field
2) Apply current I_{13} and measure V_{24P}
   Apply current I_{31} and measure V_{42P}
   Repeat to measure V_{13P} & V_{31P} using I_{42} & I_{24} respectively
3) Reverse the Magnetic Field
4) Repeat step 2 to measure V_{24N}, V_{42N}, V_{13N}, & V_{31N}

Part C) Calculations

Let the following variables be defined for convenience:

$$V_C = V_{24P} - V_{24N} \qquad V_D = V_{42P} - V_{42N}$$
$$V_E = V_{13P} - V_{13N} \qquad V_F = V_{31P} - V_{31N}$$

The sample carrier type can be determined using

$$V_C + V_D + V_E + V_F \quad > 0 : \text{p-type}$$
$$< 0 : \text{n-type}$$

Sheet Carrier Density

$$p_s = \frac{8 \cdot 10^{-8} IB}{q(V_C + V_D + V_E + V_F)}$$

$$n_s = \left| \frac{8 \cdot 10^{-8} IB}{q(V_C + V_D + V_E + V_F)} \right|$$

Sheet Resistance, R_S

R_S is found by solving the equation $e^{-\rho R_A/R_S} + e^{-\rho R_B/R_S} = 1$

if $R_A \approx R_B$ then $R_S \approx \rho R/2$, however ρ is not known, otherwise it must be solved numerically.

Numeric Algorithm

1. Set a relative error of $\delta = 0.0005$

2. Calculate $z_0 = \dfrac{2\ln 2}{\pi(R_A + R_B)}$

3. Calculate $y_i = \dfrac{1}{\exp(\pi z_{i-1} R_A)} + \dfrac{1}{\exp(\pi z_{i-1} R_B)}$

4. Calculate $z_i = z_{i-1} - \dfrac{(1 - y_i)/\pi}{R_A/\exp(\pi z_{i-1} R_A) + R_B/\exp(\pi z_{i-1} R_B)}$

5. Repeat Steps 3 & 4 until $(z_i - z_{i-1})/z_i \le \delta$

6. Sheet Resistance, $R_S = 1/z_i$

Hall Mobility, $\mu_H \quad [cm^2/Vs]$

$\mu_H = 1/qn_S R_s$ or $\mu_H = 1/qp_S R_s$

The following values require the conducting layer thickness, d , to be known

Resistivity, $\rho \quad [\Omega \cdot cm]$

$\rho = R_S d$

Bulk Carrier Density, n or $p \quad [carrier/cm^3]$

$n = n_S/d$ for n-type material

$p = p_S/d$ for p-type material

Appendix B: Reactor Time Calculations

Appendix B steps through the calculation necessary to determine time required to receive a 1MeV equivalent fluence of 10^{14}, 10^{15}, and 10^{16} in silicon carbide in the CIF at OSUNRR.

Heavy Particle Collision:

Heavy particles interact in much the same manner as billiard balls. Ignoring effects due to Coulombic and strong nuclear forces, one can easily derive an expression for the maximum amount of energy imparted by two particles of differing mass using conservation of energy and momentum. The result is the following equation, where m and M are each particle's respective mass, and E is the energy of the incident particle.

$$Q_{\max} = \frac{mM}{(m+M)^2} E = C_{mass} E \tag{8}$$

The expression of the ratio of masses can be expressed as simply a constant, C_{mass}, where convenient.

The maximum energy imparted assumes a head on collision. As the incident particle collides at different angles, it will exchange less percentage of its energy. The average energy imparted in a collision between two masses is considered to be one-half of the maximum energy transferred in the collision, and is modeled by equation 9.

$$Q_{Ave} = \tfrac{1}{2} \cdot Q_{\max} \tag{9}$$

For a neutron colliding with silicon or carbon, equation 1 results in an average $C_{mass} \approx 0.104$. Energy of 30 to 40 eV is required to displace an atom from its lattice position in SiC. Neutrons below 1 keV rarely cause displacements, thus rarely contribute to displacement dose.

Monoenergetic Dose:

Dose is defined as the amount of energy imparted to a system per unit mass. For a fluence of monoenergetic particles, dose is equivalent to that fluence (ψ) times the scattering macroscopic-cross section ($\sum_s$, probability of collision and scatter per unit length), times the amount of energy imparted per collision (Q). Since the amount of energy per collision changes with the incident angle, the average energy per collision is used. Macroscopic cross section is defined to be the density of atoms times (N) times the microscopic cross section (σ_s), resulting in equation 3.

$$D = \psi \sum_s Q_{Ave} = \psi N \sigma_s C_{mass} E \tag{10}$$

Mulit-Energy Dose:

Since neutron sources are rarely monoenergetic, total dose is an integration over energy. Since the amount of energy imparted to the system is Q, Dose is an integration over dQ, which can be broken down into a constant times dE. Thus, dose is reduced as follows.

$$D = C_{mass} \int_0^\infty \psi N \sigma_s \cdot dE \tag{11}$$

The OSU Research Reactor's CIF facility has a neutron energy distribution such that neutron flux between energies of 1 eV and 10 MeV is roughly constant as $10^{12}\ \frac{n-cm}{cm^3 s}$. Since neutron energies below 1 KeV rarely contribute to the displacement dose, and

neutron population drops significantly at 10 MeV, the assumption is made that only neutrons from 10^3 to 10^7 eV contribute to dose. The assumption is also made that N stays constant since a significant quantity will not transmute in the reactor. Applying these assumptions, and using flux ($\dot{\psi}$) instead of fluence, the dose rate ($\dot{D}$) can be modeled by

$$\dot{D} = C_{mass} N \dot{\psi} \int_{10^3 eV}^{10^7 eV} \sigma_s(E) \cdot dE \,. \tag{12}$$

Thus, only the energy dependence of the microscopic scattering cross section of the material needs to be additionally known.

1MeV Equivalent Fluence:

The 1-MeV equivalent fluence is the fluence of 1 MeV neutrons that would contribute a similar amount of dose as the full spectrum fluence. Assuming steady-state conditions, so that all variables are time independent, then the 1 MeV equivalent flux is expressed by equation 13.

$$\dot{\psi}_{1MeV} = \frac{\dot{\psi}_{All} \int_{E_{low}}^{E_{high}} \sigma_s dE}{\sigma_{s@1MeV} \cdot 1MeV} \,. \tag{13}$$

The required time is then represented by the quotient of the target fluence to the flux, presented by equation 14.

$$t = \frac{\psi_{target}}{\dot{\psi}_{1MeV}} \tag{14}$$

Using the microscopic crossections from ENDF files for silicon and carbon, produces table 5 as the required times for the desired fluences.

Table 5: Reactor time requirements for target doses

Fluence	Power [kW]	Time [s]
1.00E+14	500	66.67
1.00E+15	500	666.7
1.00E+16	500	6667

Table 5 reflects the amount of time required to achieve the target fluence given the reactor is run at full power (500kW). Since neutron flux scales linearly with power, decreasing the power by a given fraction increases the required time by the reciprocal of that fraction.

Bibliography

1. Bergman, J.P., L. Storasta, F.H.C. Carlsson, S. Sridhara, B. Magnusson, and E. Janze'n. "Defects in 4H silicon carbide." *Physica* B 308-310: 675-679. (2001)

2. Bridgeman, Charles J. *Introduction to the Physics of Nuclear Weapons Effects*. Defense Threat Reduction Agency: Ft. Belvoir, Va. 2001

3. Callister, William D. Jr. *Materials Science and Engineering: An Introduction* (Fifth Ed). New York: John Wiley & Sons, Inc. 2000

4. Casady, J.B., and R. W. Johnson. "Status of Silicon Carbide (SiC) as a Wide-Bandgap Semiconductor for High-Temperature Applications: A Review." *Solid-State Electronics* Vol. 39 No. 10: 1409-1422. 1996

5. Chen, J., P. Jung, and H. Klein. "Production and recovery of defects in SiC after irradiation and deformation." *Journal of Nuclear Materials* 258-263: 1803-1808. (1998)

6. Chen, X.D., S. Fung, C. C. Ling, C. D. Beling, and M. Gong. "Deep level transient spectroscopic study of neutron-irradiated n-type 6H-SiC." *Journal of Applied Physics* Vol 94, No. 5 (September 2003)

7. Chien, C.L. and C.R. Westgate. (Eds.) *The Hall Effect and its Applications*. New York: Plenum. 1980

8. Choyke, W.J., and R.P. Devaty. "Progress in the study of optical and related properties of SiC since 1992." *Diamond and Related Materials* 6: 1243-1248. 1997

9. Cooper, James A. Jr, A. Rohatgi, A. Doolittle, P. Pirousz. *Consortium For The Development of Silicon Carbide For Electronics Applications*. AFRL-ML-WP-TR-2000-4085. WPAFB, OH: Air Force Research Laboratory. February 2000

10. Crofton, J., S.E. Mohney, J.R. Williams, and T. Isaacs-Smith. "Finding the optimum Al-Ti alloy composition for use as an ohmic contact to p-type SiC." *Solid-State Electronics* 46: 109-113. (2002)

11. Crockett, Heather C. *Characterization of the Optical and electrical Porperties of Proton-Irradiated 4H-Silicon Carbide*. MS Thesis, Air Force Institute of Technology. AFIT/GNE/ENP/02M-01. 2002

12. Dalibor, Thomas, Gerhard Pensi, Tsunenobu Kimoto, Hiroyuki Matsunami, Shankar Sridhara, Robert P. Devaty, and Wolfgang J. Choyke. "Radiation-induced defect centers in 4H silicon carbide." *Diamond and Related Materials* 6: 1333-1337. (1997)

13. Gao, Y., y. Tang, M. Hoshi, and T.P. Chow. "Improved ohmic contacts on n-type 4H-SiC." *Solid-State Electronics* 44:1875-1878. (2000)

14. Griffiths, David J. *Introduction to Quantum Mechanics*. Upper Saddle River, NJ: Prentice Hall. 1995

15. Heissenstein, H., H. Sadowski, and R. Helbig. "Defect correlated emission and electrical properties of 4H- and 6H-SiC epitaxial layers doped by nuclear transmutation doping (NTD).", *Physica* B 305-310: 702-705. (2001)

16. Hinrichsen, P. F., A.J. Houdayer, A.L. Barry, and J. Vincent. "Proton Induced Damage in SiC Light Emitting Diodes." *IEEE Transactions on Nuclear Science* Vol. 45 No. 6. (December 1998)

17. Holmes-Siedle, Andrew, and Len Adams. *Handbook of radiation effects* (Second Ed). Oxford: Oxford University Press. 2002

18. Irmscher, K. "Electrical properties of SiC: characterisation of bulk crystals and epilayers." *Materials Science and Engineering* B91-92: 358-366 (2002)

19. Johnson, Brian J., and Michael A Capano. "The effect of titanium on Al-Ti contacts to p-type 4H-SiC." *Solid-State Electronics* 47: 1437-1441. (2003)

20. Jones, Kent T. *Measurements of Neutron Induced Surface and Bulk Defects in 4H Silicon Carbide*. MS Thesis, Air Force Institute of Technology. AFIT/GNE/ENP/02M-03. 2002

21. Kakanakov, Roumen, Liliana Kassamakova, Ivan Kassamakov, Konstantinos Zekentes, Nikolay Kuznetsov. "Improved Al/Si ohmic contacts to p-type 4H-SiC." *Materials Science and Engineering* B80: 374-377. (2001)

22. Kinoshita, T., and K.M. Itoh. “Theory of the electron mobility in n-type 6H-SiC”. *Journal of Applied Physics* Vol. 85, No. 12. 15 June 1999.

23. Konishi, Ryohei, Ryuichi yasukochi, Osamu Nakatsuka, Yasuo Koide, Miki Moriyama, and Masanori Murakami. “Development of Ni/Al and Ni/Ti/Al ohmic contact materials for p-type 4H-SiC.” *Materials Science and Engineering* B98: 286-293. (2003)

24. LANL. “Map of the Nuclides.” http://t2.lanl.gov/data/map.html. 17 Mar 2004

25. La Via, F., F. Roccaforte, A. Makhtari, V. Raineri, P. Musumeci, and L. Calcagno. “Structural and electrical characterization of titanium and nickel silicide contacts on silicon carbide.” *Microelectronic Engineering* 60: 269-282. (2002)

26. Lebedev, A.A, A.M. Ivanov, and N.B. Strokan. “Radiation Resistance of SiC and Nuclear-Radiation Detectors Based on SiC-Films.” *Semiconductors* Vol. 38, No. 2: 125-147. (2004)

27. Lee, S.K, C.M. Zetterling, M. Ostling, J.P. Palmquist, and U. Jansson. “Low resistivity ohmic contacts on 4H-silicon carbide for high power and high temperature device applications.” *Microelectronic Engineering* 60: 261-268. (2002)

28. Lee, S.K, C.M. Zetterling, M. Ostling, J.P. Palmquist, H. Hogberg, and U. Jansson. “Low resistivity ohmic titanium carbide contacts to n- and p type 4h-SiC.” *Solid-State Electronics* 44: 1179-1186. (2000)

29. Lu, Weijie, William C. Mitchel, Candis A. Thornton, G.R. Landis, and W. Eugene Collins. “Carbon Structural Transitions and ohmic Contacts on 4H-SiC.” *Journal of Electronic Materials* Vol. 32 No. 5. 2003

30. Lu, Weijie, W.C. Mitchel, G.R. Landis, and T.R. Crenshaw. “Catalytic graphitization and ohmic contact formation on 4H-SiC.” *Journal of Applied Physics* Vol. 93, No. 9. May 2003

31. Marinova, Ts, A. Kakanakova-Georgieva, V. Krastev, R. Kakanakov, M. Neshev, L. kassamakova, O. Noblanc, C. Arnodo, S. Cassette, C. Brylinski, B. Pecz, G. Radnoczi, and Gy. Vincze. "Nickel Based ohmic Contacts on SiC." *Materials Science and Engineering* B46: 223-226. (1997)

32. Masri, Pierre. "Silicon carbide and silicon carbide-based structures: The physics of epitaxy." *Surface Science Reports* 48:1-51 (2002)

33. McGarrity, J.M., F.B. McLean, W.M DeLancey, J. Palmour, C. Carter, J. Edmond, and R.E. Oakley. "Silicon Carbide JFET Radiation Response." *IEEE Transactions on Nuclear Science*, Vol. 39, No. 6. (December 1992).

34. McGuire, Gary E. (Ed.) *Characterization of Semiconductor Materials, Vol 1*. Park Ridge: Noyes. 1989

35. McKelvey, John P. Solid State Physics for Engineering and Materials Science. Malabar, FL: Krieger. 1993

36. McLean, F. Barry, James M. McGarrity, Charles J. Scozzie, C. Wesley Tipton, and W. Merie DeLancey. "Analysis of Neutron Damage in High-Temperature Silicon Carbide JFETs." *IEEE Transactions on Nuclear Science*, Vol. 41, No. 6. (December 1994)

37. Messenger, George C, and Milton S. Ash. *The Effects of Radiation on Electronic Systems*, 2nd Ed. Van Nostrand Reinhold: New York. 1992

38. Metzger, S., H. Henshel, O. Köhn, and W. Lennartz. "Silicon Carbide Radiation Detector for Harsh Environments." *IEEE Transactions on Nuclear Science* Vol. 49 No. 3. (June 2002)

39. Mohney, S.E., B.A. Hull, J.Y. Lin, and J. Crofton. "Morphological study of the Al-Ti ohmic contact to p-type SiC." *Solid-State Electronics* 46: 689-693. (2002)

40. Morath, Christian P. *Electrical Characterization of Ion-Implanted 4H-Silicon Carbide*. MS Thesis, Air Force Institute of Technology. AFIT/GAP/ENP/99M-05. 1999

41. NIST, Semiconductor Electronics Division (EEEL). “Hall Effect Measurements.” n. pag. http://www.eeel.nist.gov/812/hall.html. 1 November 2003.

42. O’Connor J.R. and Smiltens, J. (Eds.). *Silicon Carbide: A High Temperature Semiconductor*. Oxford: Pergamon Press. 1960

43. Parrington, Josef R. *Nuclides and Isotopes: Chart of the Nuclides* (Fifteenth Ed.). General Electric Co: San Jose, CA. 1996

44. Pécz, B., G. Radnóczi, S. Cassette, C. Brylinski, C. Arnodo, and O. Noblanc. “TEM study of Ni and Ni_2Si ohmic contacts to SiC” *Diamond and Related Materials* 6: 1428-1431. (1997)

45. Perlado, J.M. “Behavior and computer simulation of SiC under irradiation with energetic particles.” *Journal of Nuclear Materials* 251: 98-106. (1997)

46. Petrosky, James C. *Modeling the Radiation Effects in $Hg_{1-x}Cd_xTe$ Diodes*. PhD Thesis, Rensselaer Polytechnic Institute, NY. 1995

47. Plaksin, O.A., V.A. Stepanov, H. Amekura, and N. Kishimoto. “Conductivity of SiC during neutron and proton irradiation.” *Journal of Nuclear Materials* 307-311: 1146-1151. (2002)

48. Porter, Lisa M. and Davis, Robert F. “A Critical Review of ohmic and Rectifying contacts for Silicon Carbide.” *Materials Science and Engineering* B34: 83-105. 1995

49. Putley, E.H. *The Hall Effect and Related Phenomena*. London: Butterworths. 1960

50. Roberts, John W. *Quantum Mechanical Calculations of Monoxides of Silicon Carbide Molecules*. MS Thesis, Air Force Institute of Technology. AFIT/GNE/ENP/03-09. 2003

51. Runyan, W.R. *Semiconductor Measurements and Instrumentation*. New York: McGraw-Hill. 1975

52. Scott, Michael B. *Electrical and Optical Characterization of Intrinsic and Ion-Implanted Induced Defects in 6H- and 4H-SiC*. PhD Dissertation, Air Force Institute of Technology. AFIT/DS/ENP/97-09. 1999

53. Scozzie, C.J., J.M. McGarrity, J. Blackburn, and W. M. DeLancey. "Silicon Carbide FETs for High Temperature Nuclear Environments." *IEEE Transactions on Nuclear Science* Vol. 43 No. 3. (June 1996)

54. Turner, James E. *Atoms, Radiation, and Radiation Protection* (Second Ed). New York: Wiley-Interscience. 1995

55. Vassilevski, K., K. Zekentes, K. Tsagaraki, G. Constantinidis, and I. Nikitina. "Phase formation at rapid thermal annealing of Al/Ti/Ni ohmic contacts on 4H-SiC." *Materials Science and Engineering* B80: 370-373. (2001)

56. Vassilevski, K.V., G. Constantinidis, N. Papanicolaou, N. Martin, and K. Zekentes. "Study of annealing conditions on the formation of ohmic contacts on p+ 4H-SiC layers grown by CVD and LPE." *Materials Science and Engineering* B61-62: 296-300. (1999)

57. Yano, Toyohiko, Masafumi Akiyoshi, Kohki Ichikawi, Yoshiaki Tachi, and Takayoshi Iseki. "Physical property change of heavily neutron-irradiated Si_3N_4 and SiC by thermal annealing." *Journal of Nuclear Materials* 289: 102-109. (2001)

REPORT DOCUMENTATION PAGE

Form Approved
OMB No. 074-0188

1. REPORT DATE *(DD-MM-YYYY)*	**2. REPORT TYPE**	**3. DATES COVERED** *(From – To)*
March 2004	**Master's Thesis**	Jun 2003 – Mar 2004

4. TITLE AND SUBTITLE

LOW TEMPERATURE HALL MEASUREMENTS OF NEUTRON IRRADIATED SILICON CARBIDE

5a. CONTRACT NUMBER

5b. GRANT NUMBER

5c. PROGRAM ELEMENT NUMBER

6. AUTHOR(S)

Bonavita, Angelo, M., Second Lieutenant, USAF

5d. PROJECT NUMBER

5e. TASK NUMBER

5f. WORK UNIT NUMBER

7. PERFORMING ORGANIZATION NAMES(S) AND ADDRESS(S)

Air Force Institute of Technology
Graduate School of Engineering and Management (AFIT/EN)
2950 P Street, Building 640
WPAFB OH 45433-7765

8. PERFORMING ORGANIZATION REPORT NUMBER

AFIT/GNE/ENP/04-01

9. SPONSORING/MONITORING AGENCY NAME(S) AND ADDRESS(ES)

DTRA Headquarters
Attn: Mr. Gerry Baird DTRA/CSNP
8725 John J. Kingman Road
Ft. Belvoir, VA 22060-6201 703-325-8148

10. SPONSOR/MONITOR'S ACRONYM(S)

11. SPONSOR/MONITOR'S REPORT NUMBER(S)

12. DISTRIBUTION/AVAILABILITY STATEMENT

APPROVED FOR PUBLIC RELEASE; DISTRIBUTION UNLIMITED.

13. SUPPLEMENTARY NOTES

14. ABSTRACT

The purpose of this research was to search for evidence of low temperature annealing from neutron irradiated 4H-silicon carbide. No features suggesting annealing were found below a temperature of 340K. Temperature dependant Hall effect measurements were taken over a range of 100K to 340K recording resistivity, carrier densities, and mobility. Resistivity was noted to increase with irradiation, and carrier densities appeared to decrease, while mobility appeared minimally affected by neutron irradiation. This suggests the creation of active acceptor defects decreasing carrier concentrations. N-type samples measured were 5mm x 5mm square with Nickel contacts, and irradiated to 10^{15} and 10^{16} n-cm/cm^3 of 1MeV equivalent neutron fluence. Suggestions for continuing research include using a probe station instead of wire connections to samples, use a large source current to minimize variance, and minimize cadmium shielding to reduce negative reactivity.

15. SUBJECT TERMS

Silicon Carbide, Neutron Irradiation, Hall Effect, Displacement Damage

16. SECURITY CLASSIFICATION OF:			**17. LIMITATION OF ABSTRACT**	**18. NUMBER OF PAGES**	**19a. NAME OF RESPONSIBLE PERSON**
REPORT	**ABSTRACT**	**c. THIS PAGE**			James C. Petrosky, LTC, US Army (ENP)
U	**U**	**U**	**UU**	82	**19b. TELEPHONE NUMBER** *(Include area code)* (937) 255-3636, ext 4600; e-mail: James.Petrosky@afit.edu